

# Logarithmic inimal Models

Paula Pearce, Jørgen Rasmussen

Department of Mathematics and Statistics

University of Melbourne

Parkville, Victoria 3010, Australia

Jean-Bernard Zuber

LPTHE Tour 24-25 5<sup>em</sup> étage, Université Pierre et Marie Curie { Paris 6

4 Place Jussieu, F 75252 Paris Cedex 5, France

## Abstract

Working in the dense loop representation, we use the planar Temperley-Lieb algebra to build integrable lattice models called logarithmic minimal models  $LM_{(p;p^0)}$ . Specifically, we construct Yang-Baxter integrable Temperley-Lieb models on the strip acting on link states and consider their associated Hamiltonian limits. These models and their associated representations of the Temperley-Lieb algebra are inherently non-local and not (time-reversal) symmetric. In the continuum scaling limit, they yield logarithmic conformal field theories with central charges  $c = 1 - \frac{6(p-p^0)^2}{pp^0}$  where  $p, p^0 = 1, 2, \dots$  are coprime. The first few members of the principal series  $LM_{(m; m+1)}$  are critical dense polymers ( $m = 1, c = 2$ ), critical percolation ( $m = 2, c = 0$ ) and logarithmic Ising model ( $m = 3, c = 1/2$ ). For the principal series, we find an infinite family of integrable and conformal boundary conditions organized in an extended Kac table with conformal weights  $_{r,s} = \frac{(m+1)r - ms^2 - 1}{4m(m+1)}$ ,  $r, s = 1, 2, \dots$ . The associated conformal partition functions are given in terms of Virasoro characters of (highest-weight) representations which individually decompose into a finite number of irreducible representations. We show with examples how indecomposable representations arise from fusion.

## 1 Introduction

There is much current interest [1, 2, 3, 4, 5] in Logarithmic Conformal Field Theories (LCFTs) including LCFTs in the presence of boundaries [6]. The present paper aims at studying a family of lattice integrable models, for which, it is believed, the associated conformal field theories are logarithmic. The two primary signatures of LCFTs are first the appearance of logarithmic branch cuts in correlation functions, and second and perhaps more fundamentally, the appearance of indecomposable representations of the underlying conformal algebra (Virasoro

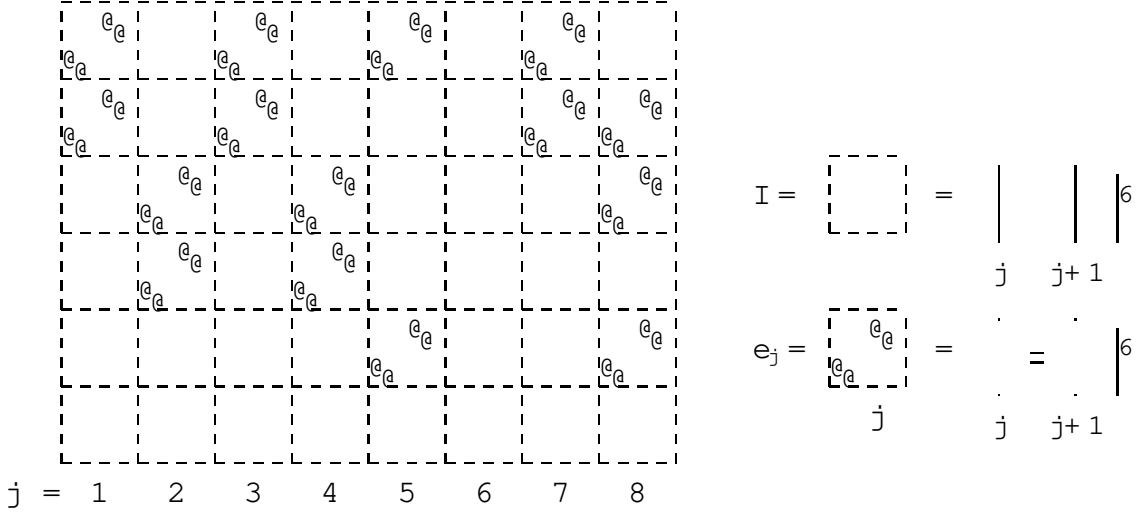


Figure 1: A simple model of critical percolation on the square lattice. Each face in a column  $j$  can be in one of two equally probable configurations which are associated with the identity  $I$  or the Temperley-Lieb generator  $e_j$ .

or one of its extensions) and their accompanying Jordan cells. On the lattice, the transfer matrix or the Hamiltonian on a strip are the precursors of the Virasoro generator  $L_0$ . To find lattice realizations of an LCFT, it is thus necessary to consider systems in which the transfer matrix is not diagonalizable and admits Jordan cells. For simple lattice models, such as the six-vertex model or RSOS models, the transfer matrices are (time-reversal) symmetric. Since these transfer matrices are real, this implies that they are diagonalizable so something different is needed.

Indecomposable representations and their associated Jordan matrices have been shown to occur in a variety of algebras: Temperley-Lieb algebra and quantum groups at roots of unity [7] and superalgebras [8, 9, 10]. This has led to supersymmetric and fermionic models [11, 12, 13, 14, 15]. In the present paper, we make use of non-local degrees of freedom.

Usually in statistical mechanics, one works with local degrees of freedom, such as spins or heights. In contrast, in other classes of physical problems [16, 17] such as percolation (see Figure 1) and polymers, one needs to keep track of connectivities or some other degrees of freedom which are inherently non-local. This shift in paradigm has a dramatic effect on the physical properties of these models. Specifically, for the models considered here, we comment that the set of exponents extends beyond [16] the "minimal Kac table" and that their associated conformal field theories are in fact logarithmic [12, 18, 19]. Indeed, it is demonstrated that the transfer matrices, although real, in some cases are not diagonalizable and hence lead to Jordan cells.

There is some evidence [20, 2, 21, 22, 23, 24] to suggest that there is an LCFT associated with each minimal model  $M_{(p,p^0)}$ . These LCFTs are in some sense the simplest LCFTs. In

this paper, we develop ideas involving non-local connectivities, the planar Temperley-Lieb (TL) algebra [25, 26] and its action on states of planar link diagrams, to build integrable lattice models which we call logarithmic minimal models  $LM(p;p^0)$ . These models might play a similar role for logarithmic theories as the Andrews-Baxter-Forrester-RSOS models [27] do for rational theories. The isotropic critical percolation model  $LM(2;3)$  is illustrated in Figure 1. The idea to use transfer matrices acting on connectivity states dates back to the early eighties [28]. The role of planar link diagrams as ideals of the TL algebra was emphasized in [29]. The approach developed here has its roots in the loop version of the  $O(n)$  model [30]. Presumably, an alternative approach could be developed by using cluster transfer matrices [31].

We assert that the continuum scaling limit of the  $LM(p;p^0)$  lattice models define logarithmic CFTs which we also call logarithmic minimal models and also denote by  $LM(p;p^0)$ . These theories offer a laboratory for studying LCFTs further by opening up new approaches to this important class of problems. In particular, these theories are amenable to study by the use of functional equations, Bethe ansatz,  $T$ -systems,  $Y$ -systems and Thermodynamic Bethe Ansatz.

We believe the main originality of the present paper lies in the use of boundary conditions in the loop model, that are consistent with integrability. It has been known for a long time [32, 33, 34] that boundary conditions are suitable to expose the representation content of a CFT and to study the fusion of these representations. Here we borrow from the work by Behrend and Pearce [35] the construction of boundary states that are solutions of the Boundary Yang-Baxter Equations (BYBEs). These boundary conditions in the conformal continuum limit are expected to give rise to representations of the Virasoro algebra. Specifically, the boundary conditions that we consider are labelled by a pair of integers  $(r;s)$  with  $(1;1)$  playing the role of the vacuum boundary condition. Imposing the boundary conditions  $(1;1)$  and  $(r;s)$  on the two sides of the strip gives rise to a certain representation  $(r;s)$ , to be defined below, of the Virasoro algebra and enables us to write an explicit form of the corresponding Hamiltonian. Imposing  $(r;s)$  and  $(r^0;s^0)$  boundary conditions gives access [34] to the fusion of representations  $(r;s)$  and  $(r^0;s^0)$ . Our model thus provides a practical tool to study the fusion of representations and to see the generation of indecomposable representations.

The layout of this paper is as follows. We start in Section 2 by summarising the spectral conformal data obtained for our logarithmic minimal models. We recall the various types of representations of the Virasoro algebra, namely, fully reducible (quotient modules) and indecomposable representations. In Appendix A, we show how the fully reducible representations decompose into a finite number of irreducible representations. In Section 3, we use the planar TL algebra to define integrable lattice realizations of the minimal LCFTs. We review the definition of the planar TL algebra [26]. We show that the lattice logarithmic minimal models are integrable in the sense that the local face operators  $X(u)$ , where  $u$  is the spectral parameter, satisfy the Yang-Baxter Equations (YBEs) and Boundary Yang-Baxter Equations (BYBEs). We also

use the construction of Behrend and Pearce [35] to obtain an infinite hierarchy of solutions to the  $YBE$  labelled by extended Kac labels  $(r; s)$  with  $r; s = 1; 2; \dots$ . In Section 4, we discuss the relation between the planar TL algebra and the more usual linear TL algebra. We introduce link diagrams which are the non-local states that keep track of connectivities. We also specialize the inversion,  $YBE$  and  $YBES$  to their appropriate forms in the linear TL algebra. In Section 5, we set up commuting double-row transfer matrices  $D(u)$  and argue that there exist integrable and conformal boundary conditions labelled by the entries of the infinite Kac table  $(r; s)$  with  $r; s = 1; 2; 3; \dots$ . Next we obtain explicit expressions for the integrable Temperley-Lieb link Hamiltonians by taking the logarithmic derivative of the commuting double-row transfer matrices  $D(u)$  at  $u = 0$ . In Section 6, we discuss the relation of the logarithmic inimimal models to the six-vertex model. We also present analytic expressions for the bulk and boundary free energies including the forms applicable in the Hamiltonian limit. In Section 7, we turn to the conformal spectra on the strip obtained in the continuum scaling limit, first restricting ourselves to the case where one boundary is the vacuum. In these cases, we find that the transfer matrices are diagonalizable and the spectrum generating functions are given by a single conformal character corresponding to a quasi-rational quotient module of the Virasoro algebra. We present numerical evidence to support this assertion. In Section 8, by considering non-trivial boundaries on both sides of the strip, we show how indecomposable representations are generated by fusion of the quotient modules. This observation is crucial in the claim that our models are logarithmic. We leave a more detailed discussion of the fusion algebras to a subsequent paper. Section 9 contains a brief discussion.

## 2 Logarithmic inimimal CFT

### 2.1 Spectral Data

The usual rational inimimal models are constructed on fully reducible highest-weight representations of the Virasoro algebra, from which one extracts a finite set of irreducible representations. The value of the central charge is specified by two coprime integers  $p; p^0$ , with  $1 < p < p^0$  and

$$c = c(p; p^0) = 1 - \frac{6(p - p^0)^2}{pp^0} \quad (2.1)$$

The conformal weights, which label the irreducible representations, are given by the Kac formula

$$r; s = \frac{(p^0 r - p s)^2 - (p - p^0)^2}{4pp^0}; \quad 1 \leq r \leq p^0; \quad 1 \leq s \leq p^0 \quad (2.2)$$

In contrast, logarithmic CFTs are constructed on representations of the Virasoro algebra which are not all fully reducible highest-weight representations: some of the representations are

$m = 1; c = 2$

$m = 2; c = 0$

$\vdots$	$\vdots$	$\vdots$	$\vdots$	$\vdots$	$\vdots$	$\ddots$
$\frac{63}{8}$	$\frac{35}{8}$	$\frac{15}{8}$	$\frac{3}{8}$	$\frac{1}{8}$	$\frac{3}{8}$	
6	3	1	0	0	1	
$\frac{35}{8}$	$\frac{15}{8}$	$\frac{3}{8}$	$\frac{1}{8}$	$\frac{3}{8}$	$\frac{15}{8}$	
3	1	0	0	1	3	
$\frac{15}{8}$	$\frac{3}{8}$	$\frac{1}{8}$	$\frac{3}{8}$	$\frac{15}{8}$	$\frac{35}{8}$	
1	0	0	1	3	6	
$\frac{3}{8}$	$\frac{1}{8}$	$\frac{3}{8}$	$\frac{15}{8}$	$\frac{35}{8}$	$\frac{63}{8}$	
0	0	1	3	6	10	
$\frac{1}{8}$	$\frac{3}{8}$	$\frac{15}{8}$	$\frac{35}{8}$	$\frac{63}{8}$	$\frac{99}{8}$	
0	1	3	6	10	15	

$\vdots$	$\vdots$	$\vdots$	$\vdots$	$\vdots$	$\vdots$	$\ddots$
12	$\frac{65}{8}$	5	$\frac{21}{8}$	1	$\frac{1}{8}$	
$\frac{28}{3}$	$\frac{143}{24}$	$\frac{10}{3}$	$\frac{35}{24}$	$\frac{1}{3}$	$\frac{1}{24}$	
7	$\frac{33}{8}$	2	$\frac{5}{8}$	0	$\frac{1}{8}$	
5	$\frac{21}{8}$	1	$\frac{1}{8}$	0	$\frac{5}{8}$	
$\frac{10}{3}$	$\frac{35}{24}$	$\frac{1}{3}$	$\frac{1}{24}$	$\frac{1}{3}$	$\frac{35}{24}$	
2	$\frac{5}{8}$	0	$\frac{1}{8}$	1	$\frac{21}{8}$	
1	$\frac{1}{8}$	0	$\frac{5}{8}$	2	$\frac{33}{8}$	
$\frac{1}{3}$	$\frac{1}{24}$	$\frac{1}{3}$	$\frac{35}{24}$	$\frac{10}{3}$	$\frac{143}{24}$	
0	$\frac{1}{8}$	1	$\frac{21}{8}$	5	$\frac{65}{8}$	
0	$\frac{5}{8}$	2	$\frac{33}{8}$	7	$\frac{85}{8}$	

$m = 3; c = 1=2$

$m = 4; c = 7=10$

$\vdots$	$\vdots$	$\vdots$	$\vdots$	$\vdots$	$\vdots$	$\ddots$
$\frac{225}{16}$	$\frac{161}{16}$	$\frac{323}{48}$	$\frac{65}{16}$	$\frac{33}{16}$	$\frac{35}{48}$	
11	$\frac{15}{2}$	$\frac{14}{3}$	$\frac{5}{2}$	1	$\frac{1}{6}$	
$\frac{133}{16}$	$\frac{85}{16}$	$\frac{143}{48}$	$\frac{21}{16}$	$\frac{5}{16}$	$\frac{1}{48}$	
6	$\frac{7}{2}$	$\frac{5}{3}$	$\frac{1}{2}$	0	$\frac{1}{6}$	
$\frac{65}{16}$	$\frac{33}{16}$	$\frac{35}{48}$	$\frac{1}{16}$	$\frac{1}{16}$	$\frac{35}{48}$	
$\frac{5}{2}$	1	$\frac{1}{6}$	0	$\frac{1}{2}$	$\frac{5}{3}$	
$\frac{21}{16}$	$\frac{5}{16}$	$\frac{1}{48}$	$\frac{5}{16}$	$\frac{21}{16}$	$\frac{143}{48}$	
$\frac{1}{2}$	0	$\frac{1}{6}$	1	$\frac{5}{2}$	$\frac{14}{3}$	
$\frac{1}{16}$	$\frac{1}{16}$	$\frac{35}{48}$	$\frac{33}{16}$	$\frac{65}{16}$	$\frac{323}{48}$	
0	$\frac{1}{2}$	$\frac{5}{3}$	$\frac{7}{2}$	6	$\frac{55}{6}$	

$\vdots$	$\vdots$	$\vdots$	$\vdots$	$\vdots$	$\vdots$	$\ddots$
$\frac{153}{10}$	$\frac{899}{80}$	$\frac{39}{5}$	$\frac{399}{80}$	$\frac{14}{5}$	$\frac{99}{80}$	
12	$\frac{135}{16}$	$\frac{11}{2}$	$\frac{51}{16}$	$\frac{3}{2}$	$\frac{7}{16}$	
$\frac{91}{10}$	$\frac{483}{80}$	$\frac{18}{5}$	$\frac{143}{80}$	$\frac{3}{5}$	$\frac{3}{80}$	
$\frac{33}{5}$	$\frac{323}{80}$	$\frac{21}{10}$	$\frac{63}{80}$	$\frac{1}{10}$	$\frac{3}{80}$	
$\frac{9}{2}$	$\frac{39}{16}$	1	$\frac{3}{16}$	0	$\frac{7}{16}$	
$\frac{14}{5}$	$\frac{99}{80}$	$\frac{3}{10}$	$\frac{1}{80}$	$\frac{3}{10}$	$\frac{99}{80}$	
$\frac{3}{2}$	$\frac{7}{16}$	0	$\frac{3}{16}$	1	$\frac{39}{16}$	
$\frac{3}{5}$	$\frac{3}{80}$	$\frac{1}{10}$	$\frac{63}{80}$	$\frac{21}{10}$	$\frac{323}{80}$	
$\frac{1}{10}$	$\frac{3}{80}$	$\frac{3}{5}$	$\frac{143}{80}$	$\frac{18}{5}$	$\frac{483}{80}$	
0	$\frac{7}{16}$	$\frac{3}{2}$	$\frac{51}{16}$	$\frac{11}{2}$	$\frac{135}{16}$	

Table 1: Lower left corner of the extended Kac table of conformal weights  $_{rs}$  for  $m = 1; 2; 3; 4$  corresponding, respectively, to critical dense polymers ( $c = 2$ ), critical percolation ( $c = 0$ ), the logarithmic Ising model ( $c = 1=2$ ), and the logarithmic tricritical Ising model ( $c = 7=10$ ). All of the distinct conformal weights occur in the first  $m$  columns.

indecomposable. In the simple class of such theories considered here, the central charges and conformal weights are as in the usual minimal models (up to the bounds on the labels  $r, s$ ), but the Virasoro generators act on some representations through Jordan cells.

To be more precise, the CFTs that will appear in the continuum limit of our lattice models have central charges and conformal weights

$$c = 1 - \frac{6}{(r-s)}; \quad 0 < r < s; \quad r,s = \frac{[r - (s-r)s^2]}{4(s-r)}; \quad r,s = 1, 2, 3, \dots \quad (2.3)$$

where  $r$  is the crossing parameter of the lattice model. Whenever  $r = s$  is rational of the form  $r = \frac{p^0 + p}{p^0}$ , where  $p, p^0$  are two coprime integers with  $0 < p < p^0$ , this central charge coincides with  $c(p; p^0)$ . The corresponding CFT is not rational nor unitary and will be denoted by  $\text{LM } (p; p^0)$ . The conformal weights lie in an infinitely extended Kac table

$$r,s = \frac{(p^0 r - p s)^2 - (p - p^0)^2}{4 p p^0}; \quad r,s = 1, 2, 3, \dots \quad (2.4)$$

While  $s$  varies over an infinite range, it may be necessary to restrict the values of  $r$  according to the model.

The most studied LCFTs so far are models with central charges  $c = c(1; p^0)$  [20, 2, 21, 24]. In the present paper, our primary focus is the series  $\text{LM } (m; m+1)$  with central charges

$$c = 1 - \frac{6}{m(m+1)}; \quad m = 1, 2, 3, \dots \quad (2.5)$$

called the principal series and we restrict  $r$  to the range  $1 < r < m$ . The first few members of the principal series are of particular significance since they include critical dense polymers ( $m = 1, c = 2$ ) and critical percolation ( $m = 2, c = 0$ ). The other members of the series are new lattice models. Borrowing nomenclature from the usual rational models, we call them the logarithmic Ising model ( $m = 3, c = 1/2$ ), the logarithmic tricritical Ising model ( $m = 4, c = 7/10$ ) and so on. The conformal weights of these models are shown in Table 1. Despite the nomenclature, the properties of these models are actually very different from their rational cousins.

It is observed that all of the distinct conformal weights fall in the first  $m$  columns of the extended Kac table of  $\text{LM } (m; m+1)$ . This follows from a simple combination of the symmetries  $r+kp; s+kp^0 = r; s = p - rp^0$  with  $k \in \mathbb{Z}$ . In the logarithmic theories, these symmetries merely express the coincidence of conformal weights and do not indicate the identification of representations.

Specifying the central charge and conformal weights may not uniquely determine a LCFT. It is conceivable that two LCFTs could have the same spectral data but differ in their Jordan cell structures. Thus, we do not claim any exhaustive classification of LCFTs, nor do we claim that the logarithmic minimal models exhaust the LCFTs of any given central charge. Instead,

we pragmatically define minimal LCFTs as the continuum scaling limits of our logarithmic minimal models, which are well-defined integrable lattice models, and then study their conformal properties.

## 2.2 Quasi-Rational Representations and Characters

The concepts of rational conformal theory, with its finite number of representations of the chiral algebra, and of the fusion of these representations are quite familiar. The logarithmic minimal models, on the other hand, possess a countably infinite number of representations. We anticipate that the logarithmic minimal models are quasi-rational in the sense that the fusion of any two representations produces only a finite number of such representations. The representations of such a theory will be called quasi-rational, following Nahm [36], who gave a criterion for quasi-rationality.

For any rational or irrational value of  $c$  and for any positive integers  $r, s$ , the module (representation)  $V_{r,s}$  of the Virasoro algebra of highest weight  $_{r,s}$  given by (2.4) is fully reducible; it has a submodule  $V_{r,s}$  of highest weight  $_{r,s} = _{r,s} + rs$ . The character of the quotient module  $Q_{r,s} = V_{r,s}/V_{r,s}$  is

$$_{r,s}(q) = q^{c=24} \frac{q^{r,s} - q^{r,s}}{q^{\frac{1}{1}}(1 - q^n)} = q^{c=24} \frac{q^{r,s}(1 - q^{rs})}{q^{\frac{1}{1}}(1 - q^n)} \quad (2.6)$$

Such quotients  $Q_{r,s}$ , which we also denote by  $(r,s)$ , are irreducible for (generic) irrational values of  $c$ , while they are not if  $c = \frac{p^0 - p}{p^0}$  is rational. In our construction, the spectrum depends on the free parameter  $c$  and we find it varies continuously with  $c$ . This supports our assertion that the characters  $_{r,s}(q)$  above are the appropriate building blocks to describe the conformal spectra of the logarithmic minimal models LM  $(p; p^0)$ , even though  $c = \frac{p^0 - p}{p^0}$  is rational and the associated characters are not irreducible. In Appendix A, we show that the representations  $(r,s)$  decompose into a finite number of irreducible representations of the Virasoro algebra.

The characters  $_{r,s}(q)$  arise as the limit of finite characters for a lattice strip of  $N$  columns

$$_{r,s}(q) = \lim_{N \rightarrow \infty} {}^{(N)}_{r,s}(q) \quad (2.7)$$

where

$${}^{(N)}_{r,s}(q) = q^{c=24+} \sum_{\substack{h \\ (N-s+r)=2}} \frac{h}{q^h} \sum_{\substack{i \\ q^{rs}}} \frac{i}{q^{rs}} \sum_{\substack{h \\ (N-s-r)=2}} \frac{h}{q^h} \sum_{\substack{i \\ q^i}} \frac{i}{q^i} \quad (2.8)$$

Here  $\sum_{m}^h$  is a  $q$ -binomial (Gaussian polynomial) and  $N = r + s \bmod 2$ . The dimension of the vector space of states is given by  $\dim V = {}^{(N)}_{r,s}(1)$ .

The fusion of the representations  $(r,s)$  generates new representations that may be indecomposable. For example, we will show in Section 8 that for critical dense polymers ( $m = 1$ ,

c= 2) the fusion of  $(1;2)$  with itself is

$$(1;2) \quad f \quad (1;2) = (1;1) \quad i \quad (1;3) \quad (2.9)$$

As indicated by the subscript  $i$ , the right side is not a direct sum of representations but rather an indecomposable combination exhibiting Jordan cells. Of course, since the character of the indecomposable representation is insensitive to the off-diagonal terms, it is simply  $\chi_{1;1}(q) + \chi_{1;3}(q)$ .

The closure of all these (fully reducible or indecomposable) representations under fusion constitutes the set of quasi-rational representations of the logarithmic minimal models.

### 3 Planar Temperley-Lieb Algebra

From a simple perspective, a planar algebra [26] is a closed algebra of diagrams known as planar tangles. The diagrams can be interpreted (by selecting in- and out- states) as giving rise to multiplications in different directions corresponding to a consistent action on a collection of vector spaces. Here we only consider the planar Temperley-Lieb (TL) algebra.

Given a planar algebra admitting local face operators satisfying the Yang-Baxter equation, one can build an integrable lattice model. To define integrable lattice models [37] on the square lattice which realize the minimal LCFTs LM  $(p;p^0)$  in the continuum scaling limit, we use solutions of the Yang-Baxter Equation (YBE) built from the planar TL algebra [26]  $T = T(\cdot)$  with crossing parameter  $2R$  which for LM  $(p;p^0)$  is specialized to

$$= \frac{(p^0 - p)}{p^0}; \quad p, p^0 \text{ coprime} \quad (3.1)$$

We introduce a complex spectral parameter  $u \in \mathbb{C}$  and set

$$s_r(u) = \frac{\sin(u + r)}{\sin}; \quad r \in \mathbb{Z} \quad (3.2)$$

The local face operators are defined in terms of elementary 2-boxes (monoids [38]) by

$$X(u) = \boxed{u} = \boxed{\text{ } \text{ } \text{ } \text{ }} + \boxed{\text{ } \text{ } \text{ } \text{ }} = s_1(u)X(0) + s_0(u)X(+) \quad (3.3)$$

The 2 in 2-box refers to the fact that there are 2 connectivities in and 2 connectivities out. The lower-left corner of a lattice face is marked to fix its orientation. Internally, the nodes at the centers of the edges of a face can be connected in pairs in one of two ways as specified by the two elementary 2-boxes. The weights, or unnormalized probabilities, assigned to these elementary 2-boxes are

$$W \quad \boxed{\text{ } \text{ } \text{ } \text{ } \text{ } !} = s_1(u); \quad W \quad \boxed{\text{ } \text{ } \text{ } \text{ } \text{ } !} = s_0(u) \quad (3.4)$$

We often omit the spectral parameters in the elementary 2-boxes when they are clear from context.

The usual physical requirement is that these weights are positive but it is useful here to relax this constraint. From the diagonal reflection symmetries and crossing symmetries, we have

$$X(u) = \boxed{u} = \boxed{u} = \boxed{u} = \boxed{u} \quad (3.5)$$

The face operator and elementary 2-boxes can be viewed as acting from any two adjacent nodes (in-states) to the remaining two adjacent nodes (out-states). In this manner, these operators can act in the four diagonal directions on distinct vector spaces spanned by link diagrams enumerating the allowed planar connectivities of the relevant nodes. In physical terms, the planar TL algebra is interpreted as a loop gas with fugacity

$$= 2 \cos \pi x + x^{-1}; \quad x = e^i; \quad 2(2;2) \quad (3.6)$$

assigned to each closed loop.

The elementary 2-boxes thus satisfy the simple relations

$$\begin{array}{ccc} \text{Diagram 1} & = & \text{Diagram 2} \\ \text{Diagram 3} & = & \text{Diagram 4} \end{array} \quad (3.7)$$

where the dashed lines indicate that the corners and associated incident edges are identified. Viewed as acting horizontally, these are the standard relations  $II = I$ ,  $e_j^2 = e_j$  of the linear TL algebra as in Section 4. In the planar algebra, however, these relations are valid for action in any direction, horizontally or vertically.

### 3.1 Inversion and Yang-Baxter Equations

Let us prove the inversion and Yang-Baxter relations in the planar TL algebra. Diagrammatically, the inversion relation is

$$\begin{array}{c} \text{Diagram 1} \\ \text{Diagram 2} \end{array} = \begin{array}{c} \text{Diagram 3} \\ \text{Diagram 4} \end{array} + \begin{array}{c} \text{Diagram 5} \\ \text{Diagram 6} \end{array} + \begin{array}{c} \text{Diagram 7} \\ \text{Diagram 8} \end{array} + \begin{array}{c} \text{Diagram 9} \\ \text{Diagram 10} \end{array} = s_1(u)s_1(-u) \begin{array}{c} \text{Diagram 11} \end{array} \quad (3.8)$$

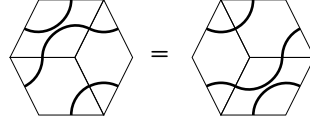
The cancellation of the three omitted terms follows from the trigonometric identity between their weights

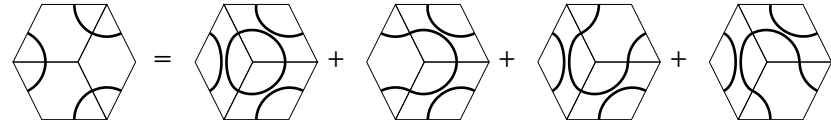
$$s_1(-u)s_0(-u) + s_0(u)s_1(u) + s_0(u)s_0(-u) = 0 \quad (3.9)$$

The Yang-Baxter equations express the equality of two planar tangles

$$\begin{array}{ccc} \text{Diagram 12} & = & \text{Diagram 13} \\ \text{Diagram 14} & & \text{Diagram 15} \end{array} \quad (3.10)$$

Allowing for the five possible connections of the external nodes, this reduces to the diagrammatic equations


(3.11)

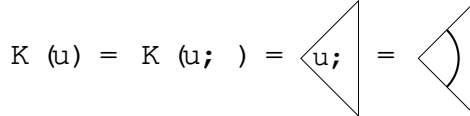

(3.12)

The first equation, which is a trivial identity, occurs three times under rotations through  $120^\circ$ . The second equation occurs twice under rotations through  $180^\circ$ . Setting  $w = v - u$ , the second equation follows from the trigonometric identity

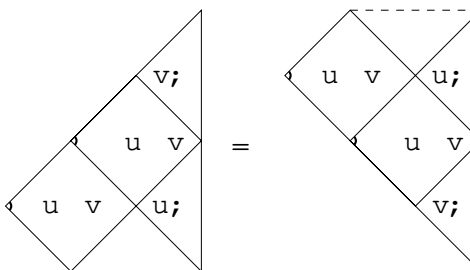
$$\begin{aligned} s_1(-u)s_0(v)s_1(-w) &= s_0(u)s_1(-v)s_0(w) + s_0(u)s_1(-v)s_1(-w) \\ &\quad + s_1(-u)s_1(-v)s_0(w) + s_0(u)s_0(v)s_0(w) \end{aligned} \quad (3.13)$$

### 3.2 Boundary Triangles and Boundary YBE

To incorporate boundaries, we introduce 1-triangles. An elementary 1-triangle with no internal degrees of freedom is defined by


(3.14)

where  $\cdot$  is a fixed boundary parameter which is often suppressed. The 1 in 1-triangle refers to the fact that there is 1 connectivity in and 1 connectivity out. This boundary condition, which we label by  $(r;s) = (1;1)$ , will play the role of the vacuum boundary condition. For given boundary 1-triangles, the Boundary Yang-Baxter Equations (BYBEs) express the equality of the two boundary tangles


(3.15)

For the elementary 1-triangle, for example, this follows from the following four identities where equality applies to connectivities as well as weights

(3.16)

### 3.3 Braids

The planar TL algebra extends to a planar braid-monoid (tangle) algebra by adding braid 2-boxes. The braid 2-boxes are defined by braid limits of the face operators

$$b = k \lim_{u \rightarrow 0^+} \frac{X(u)}{s_1(-u)} = \begin{array}{|c|c|} \hline & | \\ | & | \\ & | \\ \hline \end{array}; \quad b^{-1} = k^{-1} \lim_{u \rightarrow 0^+} \frac{X(u)}{s_1(-u)} = \begin{array}{|c|c|} \hline | & | \\ & | \\ | & | \\ \hline \end{array} \quad (3.17)$$

Although the constant  $k$  is arbitrary, the choice  $k = -i x^{1/2} = -i x^{-1/2}$  is compatible with crossing symmetry since then

$$b = -i x^{1/2} X(0) \quad X^{1/2} X(0); \quad b^{-1} = -i x^{-1/2} X(0) \quad X^{1/2} X(0) \quad (3.18)$$

and

$$X(u) = \frac{x^{1/2} e^{iu} b + x^{1/2} e^{-iu} b^{-1}}{i(x - x^{-1})}; \quad X(-u) = \frac{x^{1/2} e^{iu} b^{-1} + x^{1/2} e^{-iu} b}{i(x - x^{-1})} \quad (3.19)$$

There are many relations that hold in the planar TL braid-monoid algebra. The braid relations

(3.20)

for example, follow immediately by taking the limit  $u;v;v \rightarrow 0^+$  in the YBE. The inverse relation

(3.21)

follows by taking  $u = 1$  in the inversion relation. The twist relation is

$$\text{Diagram 1} = ! \text{ (diamond)}; \quad ! = \text{ix}^{3=2} \quad (3.22)$$

Another relation, which we will need later, is the rotated partner of (3.21) with a spectator 1+triangle

$$\begin{array}{c} \text{Diagram 1} \\ \text{Diagram 2} \end{array} = \begin{array}{c} \text{Diagram 3} \end{array} \quad (3.23)$$

### 3.4 Integrable and Conformal Boundary Conditions

In this section, we start with the vacuum boundary condition and use the fusion construction of Behrend and Pearce [35] to build an infinite family of solutions to the B Y B E labelled by Kac labels  $(r; s)$  with  $r, s = 1, 2, \dots$ . The  $(r; s)$  integrable boundary condition leads to the  $(r; s)$  conformal boundary condition in the continuum scaling limit. The construction process is valid in the planar Temperley-Lieb algebra. Since the arguments are formally the same as in [35], we just summarize the relevant results.

The  $(r;s)$  solution is built in a two-stage process as the fusion product  $(r;1) \circ_f (1;s)$  of integrable seams  $s$  acting on the vacuum  $(1;1)$  1-triangle. It is represented by the 1-triangle

$$\begin{array}{c|c}
 (r; s) & (r; 1) & (1; s) \\
 \hline
 \begin{array}{c} u; \\ A \\ A \\ A \\ A \end{array} & \begin{array}{c|c|c|c|c|c|c}
 u & r_2 & u & r_3 & & & u & 0 \\ \hline
 u & r_1 & u & r_2 & & & u & 1
 \end{array} & \cdots
 \end{array} = \begin{array}{c|c}
 & \begin{array}{c} i1 \\ A \\ A \\ A \\ A \\ \cdots \end{array} \\
 \hline
 & \cdots
 \end{array} \quad (3.24)$$

$\{z\}$

$r \quad 1 \text{ columns}$

Here there are  $r = 1$  double columns of faces, the column inhomogeneities are

$$_k = + k \quad (3.25)$$

and the left edges on the left- and right-hand sides are identified. The solid dots indicate that a projector  $P^r$ , defined below, is applied along the bottom (or equivalently top and bottom) edges of the right-hand side. Any residual degrees of freedom (connectivities) on these edges are regarded as internal to the boundary.

The projectors  $P^r$ , which act on the top and the bottom, are given by

$$P^r / \sim = \dots$$

These projectors are normalized to satisfy  $(P^r)^2 = P^r$  and act on  $r-1$  strings to kill any diagram with closed half arches, that is, where any two of the  $r-1$  strings are connected. For  $\tau = \text{irrational}$ , there are an infinite number of projectors labelled by  $r = 1; 2; 3; \dots$ . However, for  $\tau = \text{rational}$ , some projectors may diverge as is clear from (4.23). For the principal series, we restrict to  $1 \leq r \leq m$  ensuring the existence of the normalized projectors.

For  $s = m$ , the  $(1;s)$  solution is given by the braid limit of the  $(s;1)$  solution

$$\begin{array}{c} (1;s) \\ \triangle \end{array} = \lim_{! \rightarrow 1l} \begin{array}{c} (s;1) \\ \triangle \end{array} = \begin{array}{c} (1;1) \\ \square \end{array} \quad (3.27)$$

$\{z\}$ 
  
 $s \quad 1 \text{ columns}$

and a similar expression with underpasses replacing overpasses on the right side of the equation for  $\langle \dots \rangle + i \langle \dots \rangle$ . The solid dots indicate that a projector  $P^s$  is applied along the row. The limits exist provided the face operators are suitably normalized. Repeatedly applying (3.23) to either braid limit it gives

showing that the  $s = 1$  rightmost strings pass straight through the boundary tangle. For  $s > m$ , we define the  $(1; s)$  boundary condition by the right side of (3.28) with  $s = 1$  columns with no

projector but the action is restricted to the vector space of link states  $V^{(s)}$  as explained in the next section. For  $s = m$ , the two definitions are equivalent. The effect of the  $(1;s)$  boundary condition is to close the  $' = s - 1$  defects on the right boundary as indicated in Figure 2 and discussed in the following.

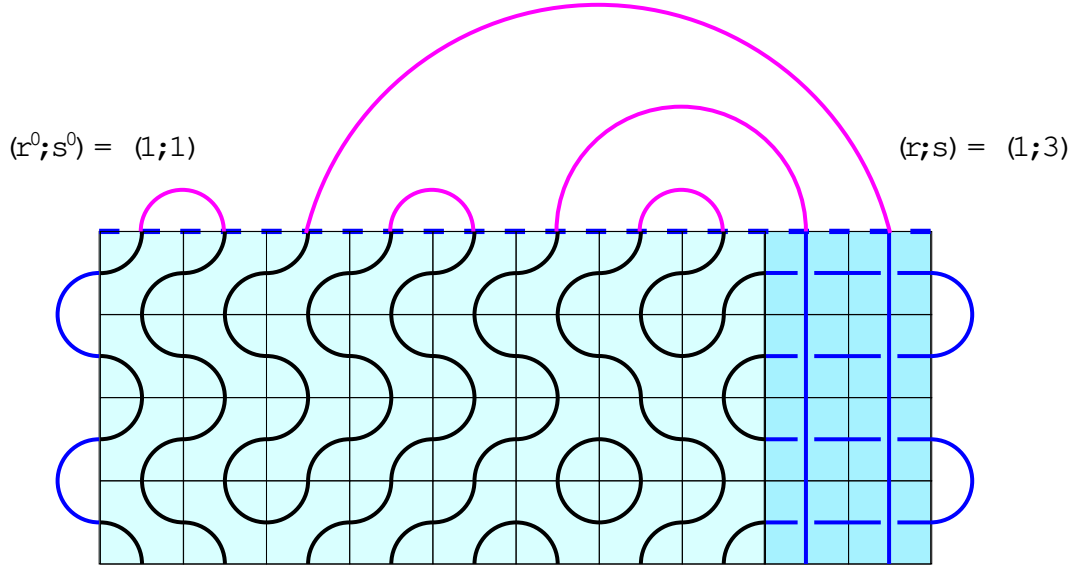


Figure 2: A typical configuration on the strip showing connectivities. The action on the link state is explained in the next section. The boundary condition is of type  $(r^0; s^0) = (1;1)$  on the left and type  $(r; s) = (1;3)$  on the right so there are  $' = s - 1 = 2$  defects in the bulk. The strings propagating along the right boundary are spectators connected to the defects.

### 3.5 Boundary Crossing

Since all closed half-arcs are projected out by the fusion projector, it follows that the normalized  $(r;1)$  boundary tangle is

$$\begin{array}{c} (r;1) \\ \triangle(u; \quad) \end{array} = \begin{array}{c} \text{Diagram with } r \text{ columns} \\ \text{and } z \text{ rows} \end{array} \quad \frac{s_{r-1}(0)s_0(2u)}{s_0(+u)s_0(-u)} \begin{array}{c} \text{Diagram with } r \text{ columns} \\ \text{and } z \text{ rows} \end{array} \quad (3.29)$$

This is a combination of equations (2.29) and (2.30) of [35]. The closed loop which is implicitly present in the second term has been cancelled against a factor  $\frac{1}{2}$  in the prefactor. Notice that only the first term, which is an  $s$ -type boundary condition of type  $(1;r)$ , survives in the braid limit  $r \rightarrow 1$ .

The boundary crossing relation follows readily

$$\begin{aligned}
 \frac{1}{s_0(2u)} \begin{array}{c} \text{diamond} \\ \diagup 2u \quad \diagdown u; \end{array} &= \frac{s_2(-2u)}{s_0(2u)} \begin{array}{c} \text{diamond} \\ \diagup \text{curve} \quad \diagdown \text{curve} \end{array} + \frac{s_{-1}(2u)}{s_0(2u)} \begin{array}{c} \text{diamond} \\ \diagup \text{curve} \quad \diagdown \text{curve} \end{array} ! \begin{array}{c} \text{triangle} \\ \diagup u; \end{array} \\
 &= s_1(-u) s_{-1}(+u) \begin{array}{c} \text{grid} \\ \text{r-1 columns} \\ \{z\} \end{array} s_{r-1}(0) s_2(-2u) \begin{array}{c} \text{grid} \\ \text{r-1 columns} \\ \{z\} \end{array} \\
 &= \begin{array}{c} \text{triangle} \\ \diagup u; \end{array} \tag{3.30}
 \end{aligned}$$

Here we used the identities

$$s_2(-2u) + s_{-1}(2u) = s_0(2u) \tag{3.31}$$

$$s_0(+u) s_{-1}(-u) s_{-1}(0) s_1(2u) = s_1(-u) s_{-1}(+u) \tag{3.32}$$

## 4 Linear Temperley-Lieb Algebra

The linear Temperley-Lieb algebra [25]  $T = T(n; \cdot)$ , with  $n \geq 0$  and  $\cdot \in \mathbb{R}$ , is obtained by fixing the in- and out-states (or direction of transfer) of the planar TL algebra. The linear TL algebra thus acts on a fixed (distinguished) vector space and is generated by the identity  $I$  and the operators  $e_1, \dots, e_{n-1}$  satisfying for  $j, k = 1, 2, \dots, n-1$

$$\begin{aligned}
 e_j^2 &= e_j; & = 2 \cos \\
 e_j e_k e_j &= e_j; & \text{if } k \neq j-1 \\
 e_j e_k &= e_k e_j; & \text{if } k > j-1
 \end{aligned} \tag{4.1}$$

Here we work in the dense loop representation of the TL algebra and represent the TL generators  $e_j$  graphically by monoids [38] acting on  $n$  strings

$$e_j = \begin{array}{c} | \quad | \quad \dots \quad | \quad | \quad | \quad \dots \quad | \quad | \quad | \\ 1 \quad 2 \quad \dots \quad j-1 \quad j \quad j+1 \quad j+2 \quad \dots \quad n-1 \quad n \end{array} \tag{4.2}$$

$$\begin{aligned}
 e_j^2 &= \begin{array}{c} | \quad | \quad \dots \quad | \quad | \quad | \\ j \quad j+1 \end{array} = \dots = e_j \\
 &= \dots = \begin{array}{c} | \quad | \quad \dots \quad | \quad | \quad | \\ j \quad j+1 \end{array}
 \end{aligned} \tag{4.3}$$

For  $\epsilon \neq 0$ ,  $\epsilon^{-1}e_j$  and  $\epsilon^{-1}e_j$  are orthogonal projectors.

The number  $C_n$  of independent words  $w$  of  $T(n)$  is given by the Catalan numbers

$$C_n = \frac{2n}{n} \cdot \frac{2n}{n-1} = \frac{1}{n+1} \cdot \frac{2n}{n} = 1; 2; 5; 14; \dots; \quad n = 1; 2; 3; 4; \dots \quad (4.5)$$

The words of the linear TL algebra are divided into equivalence classes by the number of strings or defects 'passing from the bottom to the top of the monoid diagrams. For  $n = 4$ , for example, we have  $T = S_0 \sqcup S_2 \sqcup S_4$  with

$$\begin{aligned}
 ' = 0 : \quad S_0 &= f e_1 e_3; e_1 e_3 e_2; e_2 e_1 e_3; e_2 e_1 e_3 e_2 g \\
 ' = 2 : \quad S_2 &= f e_1; e_2; e_3; e_1 e_2; e_2 e_1; e_2 e_3; e_3 e_2; e_1 e_2 e_3; e_3 e_2 e_1 g \\
 ' = 4 : \quad S_4 &= f I g
 \end{aligned} \tag{4.6}$$

Under the action of the generators of the TL algebra, the defects can hop by two sites ( $e_1 \mapsto e_2 e_1$  for example) or adjacent defects can be annihilated in pairs ( $e_3 \mapsto e_1 e_3$  for example). It follows that the action of the TL algebra is block triangular on the classes  $S$ , and that  $T = T(n; \cdot)$  admits the subalgebras

$$T^* = \begin{bmatrix} & S^*; & 0 & \end{bmatrix} \quad n \quad (4.7)$$

$S^* = \begin{bmatrix} 0 & 1 & \dots & 0 \\ \vdots & \vdots & \ddots & \vdots \\ 0 & 0 & \dots & 0 \end{bmatrix} = 0 \bmod 2$

## 4.1 Link Diagrams

The  $\mathbb{Z}_2$ -valued vector space of states of the linear TL algebra is described by connectivities. However, arbitrary connectivities cannot occur. Referring to the top edge of Figure 1, it is seen that connectivity in neighbouring pairs  $\dots \cdot \cdot \cdot \cdot \cdot \cdot \cdot \dots$   $\dots \dots \dots \dots \dots \dots \dots$  is always allowed. This connectivity state will play the role vacuum for our theories. Other allowed connectivities are generated by the action of the TL algebra on the vacuum state and are described algebraically by right ideals and diagrammatically by planar link diagrams.

Let us consider the action of the TL algebra on the vector space of right ideals

$$V = V(n; \cdot) = \hbar w T : w 2 T = T(n; \cdot) i; \quad w T = f w t : t 2 T g \quad (4.8)$$

where  $h::i$  denotes the linear span. In the loop representation, each right ideal admits a graphical representation as a (planar) link diagram. For  $n = 4$ , for example, there are six right

ideals organized by the number of defects ':

$$\begin{aligned}
 ' = 0 : \quad e_2 e_1 e_3 T &= f e_2 e_1 e_3; e_2 e_1 e_3 e_2 g = \begin{smallmatrix} & & & \\ & & & \\ & & & \\ 1 & 2 & 3 & 4 \end{smallmatrix} \\
 ' = 0 : \quad e_1 e_3 T &= f e_1 e_3; e_1 e_3 e_2 g = \begin{smallmatrix} & & & \\ & & & \\ 1 & 2 & 3 & 4 \end{smallmatrix} \\
 ' = 2 : \quad e_1 T &= f e_1; e_1 e_2; e_1 e_2 e_3; e_1 e_3; e_1 e_3 e_2 g = \begin{smallmatrix} & & & \\ & & & \\ 1 & 2 & 3 & 4 \end{smallmatrix} \\
 ' = 2 : \quad e_2 T &= f e_2; e_2 e_1; e_2 e_3; e_2 e_1 e_3; e_2 e_1 e_3 e_2 g = \begin{smallmatrix} & & & \\ & & & \\ 1 & 2 & 3 & 4 \end{smallmatrix} \\
 ' = 2 : \quad e_3 T &= f e_3; e_3 e_2; e_3 e_1; e_3 e_2 e_1; e_3 e_1 e_2 g = \begin{smallmatrix} & & & \\ & & & \\ 1 & 2 & 3 & 4 \end{smallmatrix} \\
 ' = 4 : \quad IT = T &= \begin{smallmatrix} & & & \\ 1 & 2 & 3 & 4 \end{smallmatrix}
 \end{aligned} \tag{4.9}$$

The TL generators act on these link diagrams from below. We denote by  $V_s$  the vector space of right ideals with exactly  $' = s - 1$  defects. Defects occur with a fixed parity given by  $n \equiv ' \pmod{2}$ . Since defects can be annihilated in pairs but not created by the TL generators, the action of the TL generators is upper block triangular on the vector spaces  $V_s$ . The dimension of the space  $V_s$  is

$$\dim V_s = \binom{n}{s} = \frac{n}{\frac{n}{2}}, \quad \frac{n}{\frac{n}{2} - 2} \tag{4.10}$$

It is often convenient to encode the right ideals by Restricted Solid-On-Solid (RSOS or Dyck) paths  $\mathbf{p}_i = (a_0; a_1; \dots; a_n)$  where  $a_0 = a_n = 0$  and  $a_j$  is the number of half-loops above the midpoint between strings  $j$  and  $j+1$  and  $\mathbf{p}_{j+1} - \mathbf{p}_j = 1$  for each  $j = 0; 1; \dots; n - 1$ . For  $n = 6$ , we have

$$V_0 = h(0; 1; 2; 3; 2; 1; 0); (0; 1; 2; 1; 2; 1; 0); (0; 1; 0; 1; 2; 1; 0); (0; 1; 2; 1; 0; 1; 0); (0; 1; 0; 1; 0; 1; 0) \tag{4.11}$$

The action of a single TL generator  $e_j$  maps one right ideal into a scalar multiple of another right ideal. It is instructive to write down matrices representing the action of TL generators on the basis of right ideals. For  $n = 6$ , the action of  $e_1$  and  $e_2$  on  $V_0$ , for example, is given by

$$e_1 = \begin{matrix} 0 & 0 & 0 & 0 & 0 & 0 & 1 \\ B & 0 & 0 & 0 & 0 & 0 & C \\ @ & 0 & 1 & 0 & 0 & 0 & A \\ 0 & 0 & 0 & 0 & 0 & 0 & \\ 1 & 0 & 0 & 1 & & & \end{matrix}; \quad e_2 = \begin{matrix} 0 & 0 & 0 & 0 & 0 & 1 \\ B & 1 & & 0 & 0 & C \\ @ & 0 & 0 & 0 & 0 & 0 \\ 0 & 0 & 0 & 1 & & A \\ 0 & 0 & 0 & 0 & 0 & 0 & \end{matrix} \tag{4.12}$$

where the order of the basis is as given in (4.11). In general, these matrices are real but not symmetric with eigenvalues 0 or 1 so that  $e_j$  are projectors for  $\mathbf{p}_j \neq 0$ . We stress that these matrices are non-local in the sense that the action on all link states must be considered to write the matrix representative of a given  $e_j$ . Despite the graphical depiction of the TL generators, these matrices are not (time-reversal) symmetric. This results from the action on link states which encode the history from time 1 and explicitly breaks the time-reversal symmetry associated with local representations of TL.

Later it will be useful to restrict the action of the TL generators onto spin- $(s-1)=2$  subspaces defined by

$$V^{(s)} = \int_{\mathbb{R}^2} V_0 : f_{a_0; a_1; \dots; a_n} g = f \dots; s-1; s-2; \dots; 1; 0 g; \quad s = 1; 2; 3; \dots \quad (4.13)$$

where precisely the last  $s$  heights are fixed and  $s-1$  is the number of defects.

## 4.2 Face Operators and Local Relations

A solution of the YBE [37] is obtained by taking the local face operators of the planar TL algebra and fixing the direction of transfer

$$X_j(u) = \begin{array}{c|c} \dots & \dots \\ \dots & \dots \\ \hline \dots & u \\ \dots & \dots \\ \hline \dots & \dots \\ \hline j-1 & j & j & j+1 \end{array} = s_1(u) I + s_0(u) e_j \quad (4.14)$$

These operators act from below on the fixed vector space  $V(n; \cdot)$  between string  $j$  and  $j+1$ . It follows that the  $X_j(u)$  satisfy the operator form of the YBE

$$X_j(u) X_{j+1}(u+v) X_j(v) = X_{j+1}(v) X_j(u+v) X_{j+1}(u) \quad (4.15)$$

depicted graphically by

$$\begin{array}{c|c} \dots & \dots \\ \dots & \dots \\ \hline \dots & v \\ \dots & \dots \\ \hline \dots & u+v \\ \dots & \dots \\ \hline \dots & u \\ \dots & \dots \\ \hline \dots & \dots \\ \hline j-1 & j & j & j+1 & j+2 \end{array} = \begin{array}{c|c} \dots & \dots \\ \dots & \dots \\ \hline \dots & u \\ \dots & \dots \\ \hline \dots & u+v \\ \dots & \dots \\ \hline \dots & v \\ \dots & \dots \\ \hline \dots & \dots \\ \hline j-1 & j & j & j+1 & j+2 \end{array} \quad (4.16)$$

The local face operators also satisfy the single-site commutation relation

$$X_j(u) X_j(v) = s_1(u) s_1(v) I + s_0(u+v) e_j = X_j(v) X_j(u) \quad (4.17)$$

and hence the inversion relation

$$X_j(-u) X_j(u) = s_1(-u) s_1(u) I \quad (4.18)$$

The triangle boundary weights on the right

$$K_j(u; \cdot) = \begin{array}{c|c} \dots & \dots \\ \dots & \dots \\ \hline \dots & u; \\ \dots & \dots \\ \hline \dots & \dots \\ \hline j-1 & j \end{array} \quad (4.19)$$

must satisfy the Boundary Yang-Baxter Equation (BYBE)

$$X_j(u-v)K_{j+1}(u; )X_j(u+v)K_{j+1}(v; ) = K_{j+1}(v; )X_j(u+v)K_{j+1}(u; )X_j(u-v) \quad (4.20)$$

depicted graphically by

$$\begin{array}{ccc}
 \begin{array}{c} \dots \\ \vdots \\ v; \\ \hat{\otimes} \\ u+v \\ \hat{\otimes} \\ \hat{\otimes} \\ u; \\ \hat{\otimes} \\ u \\ \hat{\otimes} \\ \dots \\ \vdots \\ j \quad 1 \quad j \quad j+1 \end{array} & = & 
 \begin{array}{c} \dots \\ \vdots \\ u \quad v \\ \hat{\otimes} \\ \hat{\otimes} \\ \hat{\otimes} \\ u; \\ \hat{\otimes} \\ u+v \\ \hat{\otimes} \\ \hat{\otimes} \\ v; \\ \hat{\otimes} \\ \dots \\ \vdots \\ j \quad 1 \quad j \quad j+1 \end{array}
 \end{array} \quad (4.21)$$

A similar relation holds on the left boundary. Here  $C$  is an arbitrary parameter. Physically,  $C$  is a thermodynamic variable governing the boundary interactions. More specifically, it is a generalized boundary magnetic field. From the single-site commutation relation (4.17), it follows immediately that a fundamental solution of the BYBE (4.20) is given by

$$K_{j+1}(u) = I \quad (4.22)$$

It is the vacuum solution which is labelled by  $(r;s) = (1;1)$ .

Explicitly, in the linear TL algebra, the first few normalized fusion projectors are

$$P_j^1 = P_j^2 = I; \quad P_j^3 = I - \frac{1}{s_2(0)} e_j; \quad P_j^4 = I - \frac{s_2(0)}{s_3(0)} (e_j + e_{j+1}) + \frac{1}{s_3(0)} (e_j e_{j+1} + e_{j+1} e_j) \quad (4.23)$$

It is noted that the denominators vanish for certain rational values of  $r = s$ . However, this does not occur for the principal series with  $r = s = (m+1)$  in the cases under consideration where  $r = 1, 2, \dots, m$ . Using the TL algebra and the fusion projectors, it is possible [35] to systematically build further solutions  $K_j^{(r;s)}$  of the BYBE labelled by arbitrary Kac labels  $(r;s)$  with  $r,s = 1, 2, \dots$ :

$$\begin{aligned}
 K_{j+1}^{(r;s)}(u; ) &= P_{j+2}^r P_{j+r+1}^s \prod_{k=1}^{\Psi^1} X_{j+k}(u - r - k) \prod_{k=1}^{\Psi^1} X_{j+r+1}(u - r - k) \\
 &\quad X_{j+r-1}(i1) \quad X_{j+r-1}(i1) \\
 &\quad \vdots \quad \vdots \\
 &\quad X_{j+r-1}(i1) \quad X_{j+r-1}(u + r - k) P_{j+2}^r P_{j+r+1}^s
 \end{aligned} \quad (4.24)$$

depicted graphically by

$$\begin{aligned}
 K_{j+1}^{(r;s)}(u; \quad) &= \begin{array}{c} (r;s) \\ \vdots \\ u; \\ \vdots \\ j \quad j+1 \end{array} = \begin{array}{c} u+_{r-1} \\ \diagdown \\ u+_{r-2} \\ \diagdown \\ \vdots \\ \diagdown \\ u+_{1} \\ \diagdown \\ \text{il} \\ \diagdown \\ u_{1} \\ \diagdown \\ u_{r-2} \\ \diagdown \\ u_{r-1} \\ \diagdown \\ j \quad j+1 \quad j+2 \quad \dots \quad j+r \end{array} (1;s) \quad (4.25)
 \end{aligned}$$

where  $k = r + k$  and the solid dots indicate the action of the fusion projectors. The  $(1;s)$  boundary triangle  $K_{j+1}^{(1;s)}( \quad = \text{il} )$  occurring on the right side of (4.25) has itself a similar graphical depiction but with  $k = \text{il}$ ,  $r$  replaced by  $s$  and the boundary triangle omitted or equivalently acting as the identity. As in Section 3.4, for  $s > m$ , the fusion projectors are omitted and the action is simply restricted to the vector space of link states  $V^{(s)}$ .

After suitable normalization, it follows from (3.29) that the boundary weights are given in terms of projectors by

$$K_j^{(r;s)}(u; \quad) = P_{j+1}^r P_{j+r}^s \frac{s_{r-1}(0)s_0(2u)}{s_0( \quad + u)s_0( \quad - u)} P_{j+1}^r e_j P_{j+1}^r P_{j+r}^s \quad (4.26)$$

From the recursive definition of the projectors [35], it also follows that at  $u =$

$$K_j^{(r;s)}( \quad ; \quad) = P_j^{r+1} P_{j+r}^s \quad (4.27)$$

## 5 Computing Transfer Matrices and Hamiltonians

### 5.1 Double-Row Transfer Matrices on a Strip

The YBEs, supplemented by the additional local relations, are sufficient to imply commuting transfer matrices and integrability. To work on a strip with fixed boundary conditions on the

right and left, we need to work with  $N$  column  $D$ ouble-row Transfer  $M$ atrices (DTMs) [39, 40] represented schematically in the planar TL algebra by the  $N$ -tangle

As we will explain later, this schematic representation in the planar TL algebra needs to be interpreted appropriately to write  $D(u)$  in terms of the generators of the linear TL algebra and to write down its associated matrix.

Following the diagrammatic proof of [40], which is valid in the planar TL algebra, the DTM  $D(u)$  form a commuting family with  $D(u)D(v) = 0$ . Similarly, using boundary crossing (3.30) and following the diagrammatic proof of [40] yields the crossing symmetry  $D(u) = D(-u)$ . It also follows, at least for  $(r;s) = (1;s)$ , that  $D(u)$  is invariant under reflections about the vertical. Hence the eigenvectors of  $D(u)$  are either odd or even under the action of the chiral operator  $C$  that implements the left-right reflection on link states and the eigenvalues of  $D(u)$  are labelled by the quantum number  $C = \pm 1$ .

In contrast to the situation for RSO models, the  $DTM_{SD}(u)$  here are not transpose symmetric and are not normal so there is no guarantee that they are diagonalizable. Nevertheless, we conjecture that for the one-boundary cases (one non-vacuum boundary) the  $DTM_{SD}(u)$  are diagonalizable. This is supported by all of our numerics. The situation is very different, however, for the two-boundary cases (two non-vacuum boundaries) where in certain cases, as in Section 8, the transfer matrices are not diagonalizable and admit a Jordan cell structure.

## 5.2 Hamiltonian Limits

One way to take the Hamiltonian limit is to write  $D(u)$  in terms of the linear TL algebra. Given a solution  $K_j(u)$  of the right YBE and assuming  $\epsilon \neq 0$ , we define a DTM acting on  $T(N+2; \mathbb{C})$  by

$$D(u) = \sum_{j=0}^{N-1} X_j(u) K_N(u) \sum_{j=N-1}^0 X_j(u) e_1 \quad (52)$$

where the products are ordered and we have assumed the vacuum boundary condition on the left. This is the appropriate interpretation of (5.1) with the projectors  $e_1^1 e_1$  enforcing closure on the left. As is clear in the diagram (5.3), the  $(1;1)$  boundary triangle on the left is replaced

by a connection generated by the two TL generators  $e_1$ .

(5.3)

The form in (5.2) and (5.3) is the form used in our numerics.

For  $\epsilon \neq 0$ , a suitably normalized Hamiltonian  $H$  is defined by

$$H = \frac{1}{2} \sin \left. \frac{\partial}{\partial u} \log D(u) \right|_{u=0} \quad (5.4)$$

so that

$$D_{\parallel}(u) = D_{\parallel}(0) e^{2uH = \sin \theta + O(u^2)}; \quad D_{\parallel}(0); D_{\parallel}(u)] = 0 \quad (5.5)$$

Here we derive the Hamiltonian by expanding  $D(u)$  in (5.1) to first order in  $u$ . Omitting

the projectors, this can be carried out diagrammatically in the planar algebra:

$$\begin{aligned}
 D(u) &= \left( \begin{array}{|c|c|c|} \hline u & & u \\ \hline u & & u \\ \hline \end{array} \right) \Bigg| \Bigg| \frac{s_{r-1}(0)s_0(2u)}{s_0(-u)s_1(-u)} \left( \begin{array}{|c|c|c|} \hline u & & u \\ \hline u & & u \\ \hline \end{array} \right) \Bigg| \Bigg| \\
 &= s_1(-u)^{2N} \left( \begin{array}{|c|c|c|} \hline \text{Diagram 1} \\ \hline \end{array} \right) \Bigg| \Bigg| \frac{s_{r-1}(0)s_0(2u)}{s_0(-u)s_1(-u)} \left( \begin{array}{|c|c|c|} \hline \text{Diagram 2} \\ \hline \end{array} \right) \Bigg| \Bigg| \\
 &+ s_0(u)s_1(-u)^{2N-1} \left( \begin{array}{|c|c|c|} \hline \text{Diagram 3} \\ \hline \end{array} \right) \Bigg| \Bigg| + \left( \begin{array}{|c|c|c|} \hline \text{Diagram 4} \\ \hline \end{array} \right) \Bigg| \Bigg| \\
 &+ s_0(u)s_1(-u)^{2N-1} \left( \begin{array}{|c|c|c|} \hline \text{Diagram 5} \\ \hline \end{array} \right) \Bigg| \Bigg| + \left( \begin{array}{|c|c|c|} \hline \text{Diagram 6} \\ \hline \end{array} \right) \Bigg| \Bigg| \\
 &+ s_0(u)s_1(-u)^{2N-1} \left( \begin{array}{|c|c|c|} \hline \text{Diagram 7} \\ \hline \end{array} \right) \Bigg| \Bigg| + \left( \begin{array}{|c|c|c|} \hline \text{Diagram 8} \\ \hline \end{array} \right) \Bigg| \Bigg| + O(u^2) \tag{5.6}
 \end{aligned}$$

Collecting connectivities together gives

$$\begin{aligned}
 D(u) &= (1 - u \cot \theta)^{2N} + 2^{-1} \frac{u}{\sin \theta} \left( \begin{array}{|c|c|c|c|c|c|} \hline \text{Diagram 9} \\ \hline \end{array} \right) \Bigg| \Bigg| \\
 &\quad \frac{2u}{\sin \theta} \frac{s_{r-1}(0)}{s_0(-u)s_1(-u)} \left( \begin{array}{|c|c|c|c|c|c|} \hline \text{Diagram 10} \\ \hline \end{array} \right) \Bigg| \Bigg| \\
 &+ \frac{2u}{\sin \theta} \left( \begin{array}{|c|c|c|c|c|c|} \hline \text{Diagram 11} \\ \hline \end{array} \right) \Bigg| \Bigg| + \left( \begin{array}{|c|c|c|c|c|c|} \hline \text{Diagram 12} \\ \hline \end{array} \right) \Bigg| \Bigg| + O(u^2) \tag{5.7}
 \end{aligned}$$

In summary, we find

$$D(u) = I + \frac{2u}{\sin \theta} H + O(u^2) = I + \frac{2u}{\sin \theta} ( -1 - N \cos \theta ) I + H^{(r,s)} + O(u^2) \tag{5.8}$$

where, reinstating the projectors,

$$H^{(r,s)} = \sum_{j=1}^{N-1} e_j \frac{s_{r-1}(0)}{s_0(-u)s_1(-u)} P_{N+1}^r e_N P_{N+1}^s \tag{5.9}$$

This operator is understood to be acting on the vector space  $V^{(s)}$ . Each Hamiltonian in the infinite hierarchy  $H^{(r,s)}$  with  $r = 1, 2, \dots, m$  and  $s = 1, 2, \dots$  is integrable and can be solved by Bethe ansatz.

In the continuum scaling limit, the finite-size corrections to the Hamiltonian yield the dilatation Virasoro generator  $L_0$  as in (7.4).

## 6 Relation to Six-Vertex Model: Bethe Ansatz and Functional Equations

### 6.1 Six-Vertex Model

In principle, it is possible to derive the Bethe ansatz and functional equations of the logarithmic in in in al models directly using non-local connectivities. However, it is more expedient to consider the related faithful representation [41, 7, 42] of the linear Temperley-Lieb algebra given by the six-vertex model with vertex weights

$$\begin{array}{ccc}
 \text{W} \quad \begin{array}{|c|c|} \hline \uparrow & \uparrow \\ \uparrow & \uparrow \\ \hline \end{array} \quad ! & = & \text{W} \quad \begin{array}{|c|c|} \hline \downarrow & \downarrow \\ \downarrow & \downarrow \\ \hline \end{array} \quad ! = s_1(u); \quad \text{W} \quad \begin{array}{|c|c|} \hline \uparrow & \downarrow \\ \downarrow & \uparrow \\ \hline \end{array} \quad ! & = & \text{W} \quad \begin{array}{|c|c|} \hline \downarrow & \uparrow \\ \uparrow & \downarrow \\ \hline \end{array} \quad ! = s_0(u) \\
 & & \text{W} \quad \begin{array}{|c|c|} \hline \uparrow & \uparrow \\ \uparrow & \downarrow \\ \hline \end{array} \quad ! = e^{iu}; \quad \text{W} \quad \begin{array}{|c|c|} \hline \downarrow & \downarrow \\ \downarrow & \uparrow \\ \hline \end{array} \quad ! = e^{-iu}
 \end{array} \quad (6.1)$$

In the usual six-vertex model, the last two vertex weights are both 1, the model is arrow reversal symmetric and the central charge is  $c = 1$ . In contrast, the assignment of weights here preserves conservation of arrows at a vertex but breaks the arrow reversal symmetry and moves the central charge away from the fixed value  $c = 1$  to the value (2.3).

The elementary face weights acting on  $(\mathbb{C}^2)^N$  are given by

$$X_j(u) = \begin{bmatrix} & & & & \vdots \\ & & & & u \\ & & & \ddot{\otimes} & \\ & & \ddot{\otimes} & & \\ & & & \ddot{\otimes} & \\ \vdots & & & & \ddot{\otimes} \\ & & & & \\ j & & & & j+1 \end{bmatrix} = s_1(u) I + s_0(u) e_j \quad (6.2)$$

where

$$e_j = I \quad I \quad \begin{matrix} 0 & 0 & 0 & 0 & 0^1 \\ B & 0 & x & 1 & 0 \\ 0 & 1 & x & 1 & 0 \\ 0 & 0 & 0 & 0 & 0 \end{matrix} \quad I \quad I \quad (6.3)$$

with  $x = e^{i\pi}$  as above. The  $4 \times 4$  matrix acts at positions  $j$  and  $j+1$ . The elementary boundary  $K$  matrices acting from  $\mathbb{C}^2$  to  $\mathbb{C}^2$  are given by

$$K \quad \begin{array}{|c|} \hline \nearrow \curvearrowright \\ \hline \end{array} \quad ! = x^{1=2}; \quad K \quad \begin{array}{|c|} \hline \nearrow \curvearrowleft \\ \hline \end{array} \quad ! = x^{-1=2} \quad (6.4)$$

For arbitrary  $r, s$ , double-row transfer matrices  $T(u)$  for the six-vertex model with one non-trivial  $(r; s)$  boundary condition can be built using the TL algebra and fusion projectors following the prescription given above. These matrices have similar properties to the logarithmic in in in al models | they form commuting families and are diagonalizable. The number  $n$  of down arrows

is related to the number of defects ' by  $\sum_{j=1}^N 2n_j$ . These two models differ, however, in one crucial aspect. The number of down arrows is a good quantum number for the six-vertex model but the number of defects is not conserved for the logarithmic model in all models since defects can be annihilated in pairs. Consequently, the six-vertex transfer matrices are block diagonal whereas the logarithmic model transfer matrices are block triangular. It is precisely this block triangular structure that allows for the appearance of Jordan cells.

Since the six-vertex model (6.1) gives a faithful representation of the linear TL algebra it follows [41, 42] that all other representations, including the logarithmic in all models, satisfy the same Bethe ansatz and functional equations. Moreover, the eigenvalues are necessarily a subset of the six-vertex eigenvalues possibly with different multiplicities. This has been confirmed by numerics on small systems. For the purposes of calculating eigenvalue spectra, it therefore suffices to solve standard six-vertex Bethe ansatz equations [43, 44]. At present, only the Bethe ansatz for the largest eigenvalues in the cases  $(1;s)$  with  $r = 1$  have been worked out. The other cases are more complicated since they necessarily involve complex conjugate pairs of roots. Of course any mapping onto the six-vertex model will, of necessity, miss the indecomposable representations discussed in Section 8.

## 6.2 Bulk and Boundary Free Energies

As discussed in the previous subsection, for a given value of the crossing parameter  $\beta$ , the largest eigenvalues of the DTM<sub>SD</sub> ( $u$ ) in the vacuum sector with  $(1;1)\bar{j}(1;1)$  boundary conditions agree exactly at each finite size with the largest eigenvalues of the six-vertex model with open boundary conditions [44, 7]. It immediately follows that these models have the same bulk and boundary free energies. Through finite-size corrections, it also follows that these models have the same central charge.

The bulk and boundary free energies can be obtained analytically by solving the relevant inversion relations [45, 46]. The boundary free energies are derived in [47]. Here we just present the forms needed for the principal series with  $\beta = -m$  with  $m = 3, 4, \dots$ . These forms need to be modified for  $\beta > -3$ . The bulk free energy per face for  $0 < \beta < -2$  and  $-2 < \text{Re}(u) < 3 = 2$  is

$$f_{\text{bulk}}(u; \beta) = \frac{1}{\beta} \int_{-1}^{1} \frac{\cosh(\beta t) \sinh u t \sinh(\beta u)t}{t \sinh t \cosh t} dt \quad (6.5)$$

For  $-\frac{3}{2} < \text{Re}(u) < \frac{3}{2}$  and  $-2 < \text{Re}(\beta) < 3 = 2$ , the  $s$ -independent boundary free energies are given by

$$f_{\text{bdy}}(u; \beta; s) = f_{\text{bdy}}^{(r;s)}(u; \beta; s) = f_0(u; \beta) + f_r(u; \beta; s) \quad (6.6)$$

Here

$$f_0(u; \ ) = \frac{1}{2} \int_1^{\frac{3}{2}} \frac{\sinh \frac{(-3)t}{2} \sinh \frac{t}{2} \sinh u t \sinh(-u)t}{t \sinh \frac{t}{2} \cosh t} dt; \quad 0 < \ < \frac{3}{2} \quad (6.7)$$

$$f_r(u; \ ; \ ) = \frac{1}{2} \int_1^{\frac{3}{2}} \frac{\cosh \frac{(-2-r)t}{2} \cosh r t \sinh u t \sinh(-u)t}{t \sinh t \cosh t} dt; \quad 2 + r < \frac{3}{2} \quad (6.8)$$

and

$$f_1(u; \ ; \ ) = \log [s_0(+u)s_1(-u)] \quad (6.9)$$

In the Hamiltonian limit, the relevant expressions are given by the derivatives with respect to  $u$  at  $u = 0$ . The bulk free energy is

$$f_{\text{bulk}}(\ ) = \int_1^{\frac{3}{2}} \frac{\cosh \frac{(-2)t}{2} t \tanh t}{\sinh t} dt = \sin \int_1^{\frac{3}{2}} \frac{dt}{\cosh t (\cosh 2t - \cos )} \cot \quad (6.10)$$

For  $-\frac{3}{2} < \text{Re}(u) < \frac{3}{2}$  and  $-2 < \text{Re}(\ ) < 3 = 2$ , the boundary free energies are given by

$$f_{\text{bdy}}(\ ) = f_{\text{bdy}}^{(r,s)}(\ ) = f_0(\ ) + f_r(\ ; \ ) \quad (6.11)$$

Here

$$f_0(\ ) = \frac{1}{2} \int_1^{\frac{3}{2}} \frac{\sinh \frac{(-3)t}{2} \sinh \frac{t}{2} \tanh t}{\sinh \frac{t}{2}} dt; \quad 0 < \ < \frac{3}{2} \quad (6.12)$$

$$f_r(\ ; \ ) = \frac{1}{2} \int_1^{\frac{3}{2}} \frac{\cosh \frac{(-2-r)t}{2} \cosh r t \tanh t}{\sinh t} dt; \quad 2 + r < \frac{3}{2} \quad (6.13)$$

and

$$f_1(\ ; \ ) = \frac{\sin}{\sin \ \sin(+\ )} \quad (6.14)$$

These explicit integrals are needed for numerics.

## 7 Numerical Strip Partition Functions

In this section, we report some preliminary numerical results for finite-size partition functions on the strip. The logarithmic minimal models are of course Yang-Baxter integrable so ultimately all of these results should be obtainable analytically.

For  $(r,s) = (1;1)$ , finite-size sequences of numerical eigenvalues were obtained by solving the Bethe ansatz equations. These were generated for system sizes out to  $N = 40$  with  $N$  of a finite

parity. The numerical eigenvalues and numerical locations of the zeros of  $Q$  and  $T$  were checked against the values obtained by direct numerical diagonalization of the logarithmic minimal transfer matrices for system sizes up to  $N = 16$ . For  $(r;s)$  with  $r > 1$ , finite-size sequences of numerical eigenvalues were obtained by direct numerical diagonalization of the logarithmic minimal transfer matrices and Hamiltonians for system sizes up to  $N = 16$ . In both cases, the numerical sequences were extrapolated using van den Broek-Schwartz approximants [48] to extract the finite-size corrections.

We present numerical results for both the isotropic lattice and Hamiltonian limit and show that these indeed agree. Typically, because there is no need to enforce closure on the left with a TL projector, the Hamiltonian calculation gives an extra digit of precision. In presenting numerical results, the numerical errors in the last digit (indicated in parenthesis) are a subjective indication of errors.

## 7.1 Finite-Size Corrections

The partition function for a  $P = N$  strip with one non-trivial boundary condition is

$$Z_{(1;1)j(r;s)}^{(P;N)} = \text{Tr}_{D^P} (u)^P = \sum_n^X D^P(u) = \sum_n^X e^{P E_n} \quad (7.1)$$

For double-row transfer matrices, the finite-size corrections for the energies are

$$E_n = \ln D(u) = 2N f_{\text{bulk}} + f_{\text{bdy}} + \frac{2 \sin \#}{N} - \frac{C}{24} + \dots + k \quad ; \quad k = 0;1;2;\dots \quad (7.2)$$

where  $\# = \frac{u}{r;s}$ ,  $\# = \frac{u}{r;s}$  is the anisotropy angle and  $k$  labels the level in the conformal tower. Similarly, for the Hamiltonians  $H^{(r;s)}$ , the finite-size corrections for the energies are

$$E_n = N f_{\text{bulk}} + f_{\text{bdy}} + \frac{v_s}{N} - \frac{C}{24} + \dots + k \quad ; \quad k = 0;1;2;\dots \quad (7.3)$$

where  $\# = \frac{u}{r;s}$  and  $v_s = \frac{\sin \#}{r;s}$  is the "velocity of sound". For the full matrices

$$\frac{N}{v_s} H^{(r;s)} = (N f_{\text{bulk}} + f_{\text{bdy}}) I - L_0 - \frac{C}{24} \quad (7.4)$$

Since the free energies are independent of  $s$ , the same is true for a Hamiltonian, say  $H^{(1;s^0)j(1;s)}$ , with two non-trivial boundaries. In this case, however, the matrices may exhibit a non-trivial Jordan canonical form as we demonstrate in Section 8.

## 7.2 Critical Dense Polymers ( $m = 1; c = 2$ )

The first member LM  $(1;2)$  of the principal series is very interesting since it is a logarithmic CFT in the universality class of critical dense polymers [16, 11]. This model is exceptional

because  $\epsilon_j = \frac{1}{2}$  implies the loop fugacity vanishes ( $\epsilon = 0$ ) and  $\epsilon_j^2 = 0$  so that loops are forbidden. Consequently, the two orthogonal projectors  $\mathbb{I}^1 e_j$  and  $\mathbb{I}^{-1} e_j$  no longer exist and the general fusion construction of integrable boundary conditions fails. Consequently, we only consider  $r = 1$ . Nevertheless, the model is still Yang-Baxter integrable and there exists an infinite family of integrable and conformal boundary conditions labelled by  $s = 1; 2; 3; \dots$  corresponding to acting on different vector spaces of link states  $V^{(s)}$  (4.13). Remarkably, for this exceptional case, the limiting transfer matrices satisfy simple inversion identities, similar to those of the rational Ising model [37, 49], which enable the eigenvalue spectra to be calculated exactly on a finite lattice. Specifically, for  $(1; s)$  boundary conditions, we find

$$c = 2; \quad \gamma_{1,s} = \frac{(2-s)^2 - 1}{8}; \quad s = 1; 2; 3; \dots \quad (7.5)$$

and obtain the complete set of associated partitioned characters (2.8). We report these analytic results elsewhere [50]. Since this case has been solved analytically, we omit any discussion of the numerics.

### 7.3 Critical Percolation ( $m = 2; c = 0$ )

The second member  $LM(2; 3)$  of the principal series is also very interesting since it corresponds to critical percolation. In this case, the (suitably normalized) transfer matrix  $D(u)$  is a stochastic matrix and its Hamiltonian limit  $H$  is an intensity matrix [29]. As an aside, we point out that the entries of the Perron-Frobenius eigenvectors of these matrices are related [51, 29] to the counting of fully packed loop configurations with connections to alternating sign matrices.

Isotropic Lattice:

$$\begin{aligned} (r; s) = (1; 1) : Z_{(1,1)}(q) &= q^{-24} (1 + q^2 + q^3 + 2q^4 + 2q^5 + \dots); & c &= 0000000 (1) \\ (r; s) = (1; 2) : Z_{(1,2)}(q) &= q^{-24+} (1 + q + q^2 + 2q^3 + 3q^4 + \dots); & = & 0000000 (1) (7.6) \\ (r; s) = (2; 1) : Z_{(2,1)}(q) &= q^{-24+} (1 + q + q^2 + 2q^3 + \dots); & = & 0.624 (2) \end{aligned}$$

Hamiltonian Limit:

$$\begin{aligned} (r; s) = (1; 1) : Z_{(1,1)}(q) &= q^{-24} (1 + q^2 + q^3 + 2q^4 + \dots); & c &= 00000000 (1) \\ (r; s) = (1; 2) : Z_{(1,2)}(q) &= q^{-24+} (1 + q + q^2 + 2q^3 + 3q^4 + \dots); & = & 00000000 (1) \\ (r; s) = (1; 3) : Z_{(1,3)}(q) &= q^{-24+} (1 + q + 2q^2 + 2q^3 + \dots); & = & 0.33333333 (1) (7.7) \\ (r; s) = (1; 4) : Z_{(1,4)}(q) &= q^{-24+} (1 + q + 2q^2 + \dots); & = & 1.000000 (3) \\ (r; s) = (2; 1) : Z_{(2,1)}(q) &= q^{-24+} (1 + q + q^2 + 2q^3 + \dots); & = & 0.625 (2) \end{aligned}$$

## 7.4 Logarithmic Ising Model ( $m = 3$ ; $c = \frac{1}{2}$ )

Isotropic Lattice:

$$\begin{aligned}
 (r; s) = (1; 1) : Z_{(1;1)}(q) &= q^{\approx 24} (1 + q^2 + q^3 + 2q^4 + 2q^5 + \dots); & c &= 499999999(3) \\
 (r; s) = (1; 2) : Z_{(1;2)}(q) &= q^{\approx 24+} (1 + q + q^2 + 2q^3 + 3q^4 + \dots); & &= 062499999(2) \\
 (r; s) = (1; 3) : Z_{(1;3)}(q) &= q^{\approx 24+} (1 + q + 2q^2 + 2q^3 + \dots); & &= 49999999(7)(7.8) \\
 (r; s) = (1; 4) : Z_{(1;4)}(q) &= q^{\approx 24+} (1 + q + 2q^2 + \dots); & &= 1.3125(1) \\
 (r; s) = (2; 1) : Z_{(2;1)}(q) &= q^{\approx 24+} (1 + q + q^2 + 2q^3 + \dots); & &= 4999(2)
 \end{aligned}$$

Hamiltonian Limit:

$$\begin{aligned}
 (r; s) = (1; 1) : Z_{(1;1)}(q) &= q^{\approx 24} (1 + q^2 + q^3 + 2q^4 + \dots); & c &= 499999999(2) \\
 (r; s) = (1; 2) : Z_{(1;2)}(q) &= q^{\approx 24+} (1 + q + q^2 + 2q^3 + 3q^4 + \dots); & &= 062499999(2) \\
 (r; s) = (1; 3) : Z_{(1;3)}(q) &= q^{\approx 24+} (1 + q + 2q^2 + 2q^3 + \dots); & &= 5000000(1)(7.9) \\
 (r; s) = (1; 4) : Z_{(1;4)}(q) &= q^{\approx 24+} (1 + \dots); & &= 1.31249(2) \\
 (r; s) = (2; 1) : Z_{(2;1)}(q) &= q^{\approx 24+} (1 + q + q^2 + 2q^3 + \dots); & &= 5001(2)
 \end{aligned}$$

## 7.5 Logarithmic Tricritical Ising Model ( $m = 4$ ; $c = 7=10$ )

Isotropic Lattice:

$$\begin{aligned}
 (r; s) = (1; 1) : Z_{(1;1)}(q) &= q^{\approx 24} (1 + q^2 + q^3 + 2q^4 + 2q^5 + \dots); & c &= 69999(2) \\
 (r; s) = (1; 2) : Z_{(1;2)}(q) &= q^{\approx 24+} (1 + q + q^2 + 2q^3 + 3q^4 + \dots); & &= 0999993(8) \\
 (r; s) = (1; 3) : Z_{(1;3)}(q) &= q^{\approx 24+} (1 + \dots); & &= 60007(8) \\
 (r; s) = (1; 4) : Z_{(1;4)}(q) &= q^{\approx 24+} (1 + \dots); & &= 1.5002(3) \\
 (r; s) = (1; 5) : Z_{(1;5)}(q) &= q^{\approx 24+} (1 + \dots); & &= 2.8001(2) \\
 (r; s) = (2; 1) : Z_{(2;1)}(q) &= q^{\approx 24+} (1 + q + q^2 + 2q^3 + \dots); & &= 4374(1)
 \end{aligned}$$

Hamiltonian Limit:

$$\begin{aligned}
 (r; s) = (1; 1) : Z_{(1;1)}(q) &= q^{\approx 24} (1 + q^2 + q^3 + 2q^4 + \dots); & c &= 70003(4) \\
 (r; s) = (1; 2) : Z_{(1;2)}(q) &= q^{\approx 24+} (1 + q + q^2 + 2q^3 + 3q^4 + \dots); & &= 099998(3) \\
 (r; s) = (1; 3) : Z_{(1;3)}(q) &= q^{\approx 24+} (1 + \dots); & &= 59995(6) \\
 (r; s) = (1; 4) : Z_{(1;4)}(q) &= q^{\approx 24+} (1 + \dots); & &= 1.50001(2) \\
 (r; s) = (1; 5) : Z_{(1;5)}(q) &= q^{\approx 24+} (1 + \dots); & &= 2.80003(4) \\
 (r; s) = (2; 1) : Z_{(2;1)}(q) &= q^{\approx 24+} (1 + q + q^2 + \dots); & &= 437(1)
 \end{aligned}$$

## 8 Examples of Indecomposable Representations

In this section, we present simple examples to show that the fusion implied by taking non-vacuum boundary conditions on either side of the strip in some circumstances does lead to indecomposable representations of the Virasoro algebra. We hope to discuss the general fusion algebras in a future paper.

Consider the case of critical dense polymers with  $\kappa = 2$  and  $c = 2$ . As already mentioned in Section 5.1, if the double-row transfer matrix has an  $(1;s)$  boundary on one side and the vacuum on the other, then the transfer matrix appears to be diagonalizable. This is highly non-trivial because these transfer matrices are not normal matrices, but this observation is supported by numerical calculations for small sizes  $(N = 12)$ . Typically, the eigenvalues are distinct but this is not always the case for example in the Hamiltonian limit. We conjecture that in general these matrices are diagonalizable including in the Hamiltonian limit  $u \rightarrow 0$  and assume this in the following discussion.

Now let's consider the fusion

$$(1;2) \text{ } f \text{ } (1;2) = (1;1) \text{ } \cup \text{ } (1;3) \quad (8.1)$$

corresponding to having an  $(r;s) = (1;2)$  boundary on both sides of the transfer matrix. These boundary conditions on the left and right each introduce a single defect for a total of two defects. Since the defects can be annihilated in pairs by the action of the TL algebra, the transfer matrix is upper block triangular with blocks labelled by the defect number  $\gamma = 0;2$  corresponding to the  $(1;1)$  and  $(1;3)$  respectively. The nitzed partition function reads

$$Z_{(1;2) \cup (1;2)}^{(N)}(q) = q^{c=24} \text{Tr} q^{L_0^{(N)}} = (1;1)^{(N)}(q) + (1;3)^{(N)}(q) \quad (8.2)$$

but this is an indecomposable representation. To see what is going on, suppose  $N = 4$  and consider the Hamiltonian

$$H = \begin{matrix} 0 & & & & & 1 \\ & 0 & 1 & 0 & 0 & 0 \\ & B & 2 & 0 & 1 & 0 & 1 \\ & & 0 & 0 & 0 & 1 & 0 \\ & & & 0 & 0 & 1 & 0 \\ & & & & 0 & 0 & 1 \\ & & & & & 0 & 0 \end{matrix} \begin{matrix} C \\ A \\ \text{---} \\ \text{---} \\ \text{---} \\ \text{---} \end{matrix} + \frac{p}{2} I \quad (8.3)$$

acting on the five states

$$\begin{matrix} \text{---} \\ \text{---} \\ 1 & 2 & 3 & 4 \\ \text{---} \\ \text{---} \end{matrix} \quad \begin{matrix} \text{---} \\ \text{---} \\ 1 & 2 & 3 & 4 \\ \text{---} \\ \text{---} \end{matrix} \quad \begin{matrix} \text{---} \\ \text{---} \\ 1 & 2 & 3 & 4 \\ 1 & 2 & 3 & 4 \\ \text{---} \\ \text{---} \end{matrix} \quad \begin{matrix} \text{---} \\ \text{---} \\ 1 & 2 & 3 & 4 \\ 1 & 2 & 3 & 4 \\ 1 & 1 & 3 & 4 \\ \text{---} \\ \text{---} \end{matrix} \quad \begin{matrix} \text{---} \\ \text{---} \\ 1 & 2 & 3 & 4 \\ 1 & 2 & 3 & 4 \\ 1 & 1 & 1 & 4 \\ \text{---} \\ \text{---} \end{matrix} \quad (8.4)$$

A shift in the energy has been introduced to make the groundstate energy  $E = 0$ . In accord with the imposed boundary conditions in the left side of (8.1), it is useful to interpret the left defect in these link states as being closed on the left ( $\gamma = 1; s = 2$ ) and the right defect as being

closed on the right ( $\mathbf{c} = 1; \mathbf{s} = 2$ ). Similarly, on the right side of (8.1), it is useful to interpret the two defects as closing on the right ( $\mathbf{c} = 2; \mathbf{s} = 3$ ). The  $\mathbf{c} = 0$  and  $\mathbf{c} = 2$  diagonal blocks are diagonalizable with eigenvalues  $f_0; \frac{p}{8}g$  and  $f_0; \frac{p}{2}; \frac{p}{8}g$  respectively. The Jordan canonical form for  $H$  has rank-2 Jordan cells

$$H = \begin{pmatrix} 0 & 0 & p\frac{0}{8} & 1 & 0 & 0 & 1 & 0 & 0 & 0 & 1 & 0 & 0 & 0 & 0 & 1 \\ 0 & 0 & 0 & 0 & 0 & 1 & 0 & 0 & 0 & 0 & 0 & 0 & 0 & 0 & 0 & 0 \\ 0 & 0 & 0 & 0 & 0 & 0 & 0 & 0 & 0 & 0 & 0 & 0 & 0 & 0 & 0 & 0 \\ 0 & 0 & 0 & 0 & 0 & 0 & 0 & 0 & 0 & 0 & 0 & 0 & 0 & 0 & 0 & 0 \\ 0 & 0 & 0 & 0 & 0 & 0 & 0 & 0 & 0 & 0 & 0 & 0 & 0 & 0 & 0 & 0 \\ 0 & 0 & 0 & 0 & 0 & 0 & 0 & 0 & 0 & 0 & 0 & 0 & 0 & 0 & 0 & 0 \\ 0 & 0 & 0 & 0 & 0 & 0 & 0 & 0 & 0 & 0 & 0 & 0 & 0 & 0 & 0 & 0 \end{pmatrix} = L_0^{(4)} \quad (8.5)$$

This corresponds to the nitzed partition function

$$Z_{(1,2);(1,2)}^{(4)}(q) = Z_{(1,1)}^{(4)}(q) + Z_{(1,3)}^{(4)}(q) = q^{1=12} [(1 + q^2) + (1 + q + q^2)] = q^{1=12} (2 + q + 2q^2) \quad (8.6)$$

Of course, the actual eigenvalues of  $H$  only approach the integer energies indicated in the nitzed Virasoro generator  $L_0^{(N)}$  as  $N \rightarrow 1$ . We see that every eigenvalue of the  $(1,1)$  block has an exactly equal eigenvalue in the  $(1,3)$  block and that together they form a rank-2 Jordan cell. This pattern continues for larger values of  $N$  and has been checked numerically for  $N = 10$ . The fact that this is possible is consistent with the identity [50]

$$Z_{(1,3)}^{(N)}(q) = q^{1=12} \sum_{k=0}^{N-2} \frac{D_{M-k;M+k+1}}{E_{q^k}} \quad (8.7)$$

where for  $k \leq n$  the generalized  $q$ -Narayana numbers

$$D_{M-k;M+k+1} = q^{n(M+k+1)=2+n(n+1)=2} \frac{h_M h_{M+1} \dots h_{M+k+1}}{h_{M-n+1} h_{M-n+2} \dots h_{M-n+1}} \quad (8.8)$$

are fermionic in the sense that they are polynomials with non-negative coefficients [50]. We conjecture the exact form in the limit  $N \rightarrow 1$  is

$$L_0 = \begin{matrix} D \text{ iag}(0;2;3;4;4;:::) & J \\ 0 & D \text{ iag}(0;1;2;2;3;3;4;4;4;4;:::) \end{matrix} \quad (8.9)$$

This symbolic notation means that each energy  $E$  in the expansion  $Z(q) = q^{\mathbf{c}=24} \sum_E q^E$  of the characters occurs on the matrix diagonal and a rank-2 Jordan cell is formed between as many coincident pairs as possible with an entry 1 in  $J$ . All other entries of  $J$  are 0.

For critical dense polymers, we also find that for the case

$$(1;2) \text{ f } (1;4) = (1;3) \text{ i } (1;5) \quad (8.10)$$

the Jordan form of the truncated Virasoro generator  $L_0$  agrees with that of Gaberdiel and Kausch [4] to the level calculated in their paper. More generally, the  $s'(2)$  fusion rule

$$(1;s_1) \text{ f } (1;s_2) = (1;s_3) \quad (8.11)$$

$$s_3 = \frac{j_1 s_2 + 1}{s_1 + s_2} \quad s_3 \equiv 1 \pmod{2}$$

applies to the principal series whenever  $(1;s_3) \otimes (1;s_3^0) \not\cong \mathbb{Z}$  for any pairs  $s_3, s_3^0$ . If  $(1;s_3) \otimes (1;s_3^0) \cong \mathbb{Z}$  for some pair  $s_3, s_3^0$ , then there is the possibility to form an indecomposable representation. Looking numerically at many cases for different values of  $m$ , it seems that fusion yields an indecomposable representation whenever  $(1;s_3) \otimes (1;s_3^0) \cong \mathbb{Z}$ .

## 9 Discussion

We have argued that the essential new physics in our logarithmic minimal theories derives from the non-local nature of the degrees of freedom in the form of connectivities. For these models, we have exhibited an infinite family of Yang-Baxter integrable lattice models on the strip which realize logarithmic CFTs in the continuum scaling limit. We have described the spectra of these theories on the strip for an infinite family of boundary conditions labelled by  $(r;s)$  in an infinitely extended Kac table. Most importantly, we have shown how indecomposable representations arise in a consistent manner from within our lattice approach.

This paper has begun the task of organizing the zoo of logarithmic theories into families along side their rational cousins. We expect logarithmic counterparts to exist whenever there exists a braid-monoid algebra that can be extended to a planar algebra. We therefore expect that, from the lattice, it is possible to construct logarithmic dilute minimal models, logarithmic Wess-Zumino-Witten models as well as logarithmic models corresponding to higher fusions and higher rank.

Conventionally, to claim a consistent CFT, one must consider the system in other topologies, such as a cylinder or a torus [15, 52]. Obviously, there remains much work to be done.

## Appendix A Decomposition of $Q_{r;s}$ into Irreducible Representations

In this appendix, we consider the quasi-rational quotient module  $Q_{r;s} = V_{r;s} = V_{r;s}$  where  $V$  is the Verma module of highest weight  $\lambda$ . In the celebrated work [53], the embedding pattern of submodules of  $V_{r;s}$  is described based on which one can build the irreducible quotient module  $M_{r;s}$  associated to  $V_{r;s}$ . It is thus, in principle, a simple matter to determine how the quasi-rational module  $Q_{r;s}$  decomposes into irreducible modules. This decomposition is worked out explicitly in the following.

There are two possible embedding patterns. The typical one is conventionally described by

a diagram like

$$\begin{array}{ccccccc}
 & V_1 & ! & V_2 & ! & & !_j V! \\
 & \% & & & & & \\
 V_0 & & \& & \& & \& \& \\
 & \& & & & & & \\
 & V_1^0 & ! & V_2^0 & ! & & !_j^0 V!
 \end{array} \tag{A.1}$$

where an arrow from module A to module B indicates that B is a submodule of A. In this case, the irreducible modules associated to  $V_j$  and  $V_j^0$  are  $M_j = V_j = V_{j+1} + V_{j+1}^0$  and  $M_j^0 = V_j^0 = V_{j+1} + V_{j+1}^0$ , respectively, where we have used the unconventional + instead of since we reserve the notation for direct sums of spaces. The decomposition of the quotient module  $V_m = V_{m+n}$ , for example, into irreducible modules reads

$$V_m = V_{m+n} = M_m \underset{j=1}{\overset{M^1}{\longrightarrow}} M_{m+j} \quad M_{m+j}^0 \quad M_{m+n}^0 \tag{A.2}$$

Similar decompositions obviously apply to  $V_m = V_{m+n}^0$ ,  $V_m^0 = V_{m+n}$  and  $V_m^0 = V_{m+n}^0$ , and they all follow straightforwardly from (A.1). The alternative embedding pattern is described by the diagram

$$V_0 ! \quad V_1 ! \quad V_2 ! \quad !_j V \tag{A.3}$$

in which case the irreducible module associated to  $V_j$  is  $M_j = V_j = V_{j+1}$ , while the decomposition of the quotient module  $V_m = V_{m+n}$  into irreducible modules reads

$$V_m = V_{m+n} = \underset{j=0}{\overset{M^1}{\longrightarrow}} M_{m+j} \tag{A.4}$$

In either embedding pattern, we say that  $V_j$  and  $V_j^0$  appear with rank  $j$ .

Now, for any pair  $r, s$  of positive integers eventually labeling  $Q_{r,s}$ , let us write

$$r = r_0 + kp; \quad s = s_0 + k^0 p^0; \quad k, k^0 \geq 0 \tag{A.5}$$

where  $r_0, s_0$  are in the fundamental domain

$$1 \quad r_0 \quad p; \quad 1 \quad s_0 \quad p^0 \tag{A.6}$$

If  $r_0 < p$  and  $s_0 < p^0$ , the embedding pattern associated to  $Q_{r,s}$  is of the type (A.1), while it is of type (A.3) if at least one of the upper bounds is saturated (A.6), that is, if  $r_0 = p$  or  $s_0 = p^0$ . In general, the module  $V_{r,s}$  may be considered a submodule of  $V_{r_0,s_0} = V_{p, r_0, p^0, s_0}$  (if  $j \leq k^0 j$  is even) or of  $V_{r_0, p^0, s_0} = V_{p, r_0, s_0}$  (if  $j \leq k^0 j$  is odd). It is therefore a straightforward task to determine the decomposition of  $Q_{r,s}$  into irreducible modules: one merely has to identify the locations of  $V_{r,s}$  and  $V_{r, s}$  in the ambient embedding pattern. We will write the decompositions in terms of the associated characters

$$r,s \models (Q_{r,s}) = (V_{r,s}) \quad (V_{r, s}); \quad ; \models (M_{r, s}) \tag{A.7}$$

We first consider the situation where  $1 - r_0 < p; 1 - s_0 < p^0$ , in which case the embedding pattern headed by  $V_{r,s}$  looks like

$$\begin{array}{ccccc} \% & (r_1; s_1) & ! & (r_2; s_2) & ! \\ (r; s) & & \& & \& \\ \& (r_1^0; s_1^0) & ! & (r_2^0; s_2^0) & ! \end{array}$$

Suppose, for example, that  $k = k^0$ , in which case  $(r_{2n}; s_{2n}) = (r_0 + (k - k^0 + 2n)p; s_0)$ ,  $(r_{2n}^0; s_{2n}^0) = (r_0; s_0 + (k - k^0 + 2n)p^0)$ ,  $(r_{2n+1}; s_{2n+1}) = (r_0 + (k - k^0 + 2n + 1)p; p^0 - s_0)$ ,  $(r_{2n+1}^0; s_{2n+1}^0) = (r_0; p^0 - s_0 + (k - k^0 + 2n + 1)p^0)$ . In this chain, the submodule  $V_{r,s}$  appears with rank  $2k^0 + 1$  as it corresponds to  $(r; s) \neq (r_0 + (k + k^0 + 1)p; p^0 - s_0) = (r_{2k^0+1}; s_{2k^0+1})$ . The decomposition thus reads

$$V_{r,s} = \sum_{i=1}^{(irr)} \frac{X^{k^0}}{r_i; s} + \sum_{i=1}^{(irr)} \frac{X^{k^0+1}}{r_i; s_i} + \sum_{i=1}^{(irr)} \frac{X^{k^0+1}}{r_i^0; s_i^0} \quad (A.8)$$

For general  $r_0 < p; s_0 < p^0; 0 < k; k^0$ , we find

$$\begin{aligned} r_0 + kp; s_0 + k^0p^0 &= \sum_{j=1}^{2m} \frac{X^{(k+k^0)}}{r_0 + kp; s_0 + k^0p^0 + (jk - k^0 + j)p; (1 - (1)^j)s_0 + (1 - (1)^j)p^0} \\ &+ \sum_{j=0}^{(irr)} \frac{X^{(k+k^0)}}{r_0; (1 - (1)^j)s_0 + (1 - (1)^j)p^0} + \sum_{j=0}^{(irr)} \frac{X^{(k+k^0)}}{r_0; p^0 - s_0 + (k + k^0 + 1)p^0} \end{aligned} \quad (A.9)$$

The linear embedding patterns (A.3) corresponding to exactly one saturated upper bound (A.6) may be analyzed in a similar way. For general  $1 - r_0 < p; 1 - s_0 < p^0; 0 < k; k^0$ , we thus find the decompositions

$$\begin{aligned} r_0 + kp; (k^0 + 1)p^0 &= \sum_{j=0}^{m \text{ in } (2k; 2k^0 + 1)} \frac{X^{(k+k^0)}}{(1 - (1)^j)r_0 + (1 - (1)^j)p^0 = 2; (k + k^0 + 1 - j)p^0} \\ (k+1)p; s_0 + k^0p^0 &= \sum_{j=0}^{m \text{ in } (2k+1; 2k^0)} \frac{X^{(k+k^0)}}{(k + k^0 + 1 - j)p; (1 - (1)^j)s_0 + (1 - (1)^j)p^0 = 2} \end{aligned} \quad (A.10)$$

Finally, if both upper bounds are saturated, that is  $(r; s) = ((k+1)p; (k^0+1)p^0)$  where  $k; k^0 \neq 0$ , the embedding pattern is linear and the decomposition reads

$$(k+1)p; (k^0+1)p^0 = \sum_{j=0}^{m \text{ in } (k+k^0)} \frac{X^{(k+k^0)}}{(k + k^0 + 1 - 2j)p^0} = \sum_{j=0}^{m \text{ in } (k+k^0)} \frac{X^{(k+k^0)}}{p; (k + k^0 + 1 - 2j)p^0} \quad (A.11)$$

It is observed that a quasi-rational quotient module  $Q_{r,s} = V_{r,s} = V_{r,s}$  is irreducible if and only if it corresponds to a linear embedding pattern in which the submodule  $V_{r,s}$  is a proper submodule of  $V_{r,s}$ . That is, the only irreducible quasi-rational quotient modules are  $Q_{(k+1)p; s_0}$ ,  $Q_{r_0; (k^0+1)p^0}$ ,  $Q_{(k+1)p^0}$  and  $Q_{p; (k^0+1)p^0}$  where  $k; k^0 \neq 0$ .

## Acknowledgements

PAP and JR are supported by the Australian Research Council. We thank Michael Flohr for discussions at IPAM and for helpful correspondence and Hubert Saleur for useful discussions and help with the references at Saclay.

## References

- [1] V. Gurarie, [hep-th/9303160](#), Nucl. Phys. B 410, 535 (1993).
- [2] F. Rohsiepe, On reducible but indecomposable representations of the Virasoro algebra, [hep-th/9611160](#) (1996).
- [3] M. Flohr, [hep-th/9605151](#), Int. J. Mod. Phys. A 12, 1943{1958 (1997); Null vectors in logarithmic conformal field theory, [hep-th/0009137](#) (2000); M. Flohr, [hep-th/0111228](#), Int. J. Mod. Phys. A 18, 4497{4592 (2003).
- [4] M. R. Gaberdiel and H.G. Kausch, [hep-th/9604026](#), Nucl. Phys. B 477, 293{318 (1996); [hep-th/9807091](#), Nucl. Phys. B 538, 631 (1999).
- [5] M. R. Gaberdiel, [hep-th/0111260](#), Int. J. Mod. Phys. A 18, 4593{4638 (2003).
- [6] S. Moghimi Aghajani and S. Rouhani, [hep-th/0002142](#), Lett. Math. Phys. 53, 49{57 (2000); I.I. Kogan and J.F. Wallender, [hep-th/0003184](#), Phys. Lett. B 486, 353 (2000); S. Kawai and J.F. Wallender, [hep-th/0103197](#), Phys. Lett. B 508, 203 (2001); A. Bredthauer and M. Flohr, [hep-th/0204154](#), Nucl. Phys. B 639, 450{470 (2002); S. Kawai, [hep-th/0204169](#), Int. J. Mod. Phys. A 18, 4655{4684 (2003).
- [7] V. Pasquier and H. Saleur, Nucl. Phys. B 330, 523 (1990).
- [8] M. Marcu, J. Math. Phys. 21, 1277{1283; 1284{1292 (1980).
- [9] L. Rozansky and H. Saleur, Nucl. Phys. B 376, 461 (1992); Nucl. Phys. B 389, 365 (1993).
- [10] Z. M. Aassarani and D. Serban, [hep-th/9605062](#), Nucl. Phys. B 489, 603{625 (1997).
- [11] H. Saleur, [cond-mat/9111007](#), Nucl. Phys. B 382, 486 (1992); [cond-mat/9111008](#), Nucl. Phys. B 382, 532 (1992).
- [12] H.G. Kausch, Curiosities at  $c=2$ , [hep-th/9510149](#) (1995).
- [13] J. Kondrev and J.B. Marston, Supersymmetry and Localization in the Quantum Hall Effect, [cond-mat/9612223](#) (1996).

[14] E.V. Ivashkevich, cond-mat/9801183, *J. Phys. A* 32, 1691 (1999).

[15] N. Read and H. Saleur, hep-th/0106124, *Nucl. Phys. B* 613, 409 (2001).

[16] H. Saleur, *J. Phys. A* 20, 455{470 (1987).

[17] B. Duplantier, *J. Phys. A* 19, L1009{1014 (1986); H. Saleur and B. Duplantier, *Phys. Rev. Lett.* 58, 2325 (1987).

[18] J. Cardy, Logarithmic correlations in quenched random magnets and polymers, cond-mat/9911024 (1999).

[19] V. Gurarie and A.W.W. Ludwig, cond-mat/9911392, *J. Phys. A* 35, L377{384 (2002).

[20] H.G. Kausch, *Phys. Lett. B* 259, 448{455 (1991).

[21] M. Flohr, hep-th/9509166, *Int. J. Mod. Phys. A* 11, 4147{4172 (1996).

[22] P. Calabrese, M. Caselle, A. Celi, A. Pelissetto and E. Vicari, hep-th/0005254, *J. Phys. A* 33, 8155{8170 (2000).

[23] J. Rasmussen, hep-th/0405257, *Nucl. Phys. B* 701, 516{528 (2004); Jordan cells in logarithmic limits of conformal field theory, hep-th/0406110 (2004).

[24] H. Eberle and M. Flohr, Virasoro representations and fusion for generalized minimal models, hep-th/0604097 (2006).

[25] H.N.V. Temperley and E.H. Lieb, *Proc. Roy. Soc. (London) A* 322, 251 (1971).

[26] V.F.R. Jones, Planar algebras I, QA/9909027 (1999).

[27] G.E. Andrews, R.J. Baxter and P.J. Forrester, *J. Stat. Phys.* 35, 193{266 (1984); P.J. Forrester and R.J. Baxter, *J. Stat. Phys.* 38, 435{472 (1985).

[28] I.G. Enting, *J. Phys. A* 13, 3713{3722 (1980); B. Derrida, *J. Phys. A* 14, L5 (1981); H. B. Lote, M.P. Nightingale and B. Derrida, *J. Phys. A* 14, L45 (1981); H. B. Lote and M.P. Nightingale, *Physica A* 112, 405 (1982); M.P. Nightingale and H. B. Lote, *J. Phys. A* 16, L657 (1983); H. B. Lote and B.N. Nienhuis, *J. Phys. A* 22, 1415{1438 (1989).

[29] P.A. Pearce, V.R.ittenberg and J. de Gier, cond-mat/0108051 (2001); P.A. Pearce, V.R. Ittenberg, J. de Gier and B.N. Nienhuis, *J. Phys. A* 35, L661{668 (2002).

[30] B.N. Nienhuis, *Phys. Rev. Lett.* 49, 1062{1065 (1982); *J. Stat. Phys.* 34, 731{761 (1984).

[31] S-C. Chang and R. Schrock, Transfer matrices for the partition function of the Potts model on cyclic and Möbius lattice strips, cond-mat/0404524 (2004); J.L. Jacobsen and J. Salas, Transfer matrices and partition-function zeros for antiferromagnetic Potts models, cond-mat/0407444 (2004); J-F. Richard and J.L. Jacobsen, Character decomposition of Potts model partition functions I. Cyclic geometry and II. Toroidal geometry, math-ph/0605015, 0605016 (2006).

[32] J. Cardy, Nucl. Phys. B 240, 514 (1984).

[33] H. Saleur and M. Bauer, Nucl. Phys. B 320, 591 (1989).

[34] J. Cardy, Nucl. Phys. B 324, 581 (1989).

[35] R.E. Behrend and P.A. Pearce, hep-th/0006094, J. Stat. Phys. 102, 577{640 (2001).

[36] W. Nahm, hep-th/9402039, Int. J. Mod. Phys. B 8, 3693 (1994).

[37] R.J. Baxter, Exactly Solved Models in Statistical Mechanics, Academic Press, London (1982).

[38] L. Kau man, Topology 26, 395 (1987).

[39] E.K. Sklyanin, J. Phys. A 21, 2375-2389 (1988).

[40] R.E. Behrend, P.A. Pearce and D.L.O'Brien, hep-th/9507118, J. Stat. Phys. 84, 1{48 (1996).

[41] P.P. Martin, Potts models and related problems in statistical mechanics, Series on Advances in Statistical Mechanics, Volume 5, World Scientific, Singapore (1991).

[42] P.P. Kulish, J. Phys. A 36, L489{493 (2003).

[43] C.N. Yang and C.P. Yang, Phys. Rev. 150, 321; 327 (1966).

[44] F.C. Alcaraz, M.N. Barber, M.T. Batchelor, R.J. Baxter and G.R.W. Quispel, J. Phys. A 20, 6397{6409 (1987).

[45] R.J. Baxter, J. Stat. Phys. 28, 1 (1982).

[46] D.L.O'Brien, P.A. Pearce and R.E. Behrend, cond-mat/9511081, J. Phys. A 30, 2353{2366 (1997).

[47] R.Nepomuceno and P.A. Pearce, Boundary S-matrices of unitary minimal models, in preparation (2006).

[48] J.M. van den Broeck and L.W. Schwartz, *Siam J. Math. Anal.* 10, 639 (1979).

[49] D.L.O.'Brien, P.A. Pearce and S.O. Wamaar, *Physica A* 228, 63{77 (1996).

[50] P.A. Pearce and J. Rasmussen, *Solvable critical dense polymers*, in preparation (2006); *Physical combinatorics of critical dense polymers*, in preparation (2006).

[51] A.V. Razumov and Yu G. Stroganov, cond-mat/0012141, *J. Phys. A* 34, 3185 (2001).

[52] M. Flohr, hep-th/9509166, *Int. J. Mod. Phys. A* 11, 4147 (1996); M.R. Gaberdiel and H.G. Kausch, hep-th/9606050, *Phys. Lett. B* 386, 131{137 (1996); B.L. Feigin, A.M. Gainutdinov, A.M. Semikhatov and I.Yu. Tipunin, *Logarithmic extensions of minimal models: characters and modular transformations*, hep-th/0606196 (2006); Kazhdan-Lusztig dual quantum group for logarithmic extensions of Virasoro minimal models, math.QA/0606506 (2006) and further references therein.

[53] B.L. Feigin and D.B. Fuchs, *Funct. Anal. Appl.* 17, 241 (1983).